RESEARCH ARTICLE

Atmospheric circulation types controlling rainfall in the Central American Isthmus

Fernán Sáenz[1] | **Hugo G. Hidalgo[1,2]** | **Ángel G. Muñoz[3]** |
Eric J. Alfaro[1,2,4] | **Jorge A. Amador[1,2]** | **Jorge L. Vázquez-Aguirre[5]**

[1]Centre for Geophysical Research, University of Costa Rica, San José, Costa Rica

[2]School of Physics, University of Costa Rica, San José, Costa Rica

[3]International Research Institute for Climate and Society (IRI), Climate Division, Columbia University, New York, New York, USA

[4]Centre for Research in Marine Sciences and Limnology, University of Costa Rica, Montes de Oca, San José, Costa Rica

[5]Licenciatura en Ciencias Atmosféricas, Universidad Veracruzana, Veracruz, Mexico

Correspondence
Fernán Sáenz, Centre for Geophysical Research, University of Costa Rica, San José, Costa Rica.
Email: fernan.saenzsoto@ucr.ac.cr

Abstract

Rainfall mechanisms in the Central American Isthmus are controlled by complex physical interactions across spatial and temporal scales, which are reflected on the dynamics of atmospheric circulation patterns affecting the region. However, physical mechanisms and their relationships with thermodynamic distributions connected to overturning circulations remain elusive. Here, a set of six recurrent daily atmospheric patterns, or weather types (WT), is defined using a k-means++ clustering algorithm on standardized fields of Convective Available Potential Energy (CAPE) and winds at 925, 850, and 200 hPa. The relationships between these weather types, their temporal characteristics, and anomalous distributions of moisture flux divergence, equivalent potential temperature (saturated and unsaturated), and observed rainfall are used to describe physical processes controlling the latter, for all seasons. Regional observed rainfall is analysed from a set of 174 automatic stations from all countries from Mexico to Panama. By modulating vertically integrated moisture fluxes, these weather types, and the different climate drivers linked to them, control the temporal and spatial rainfall characteristics in the region, especially over the Pacific side of the isthmus. During some stages of the regional rainy season, described by two weather types, thermal anomalies in convective quasi-equilibrium characteristic of the upward branch of the Hadley cell force westerly flow over Central America, enhancing rainfall. While during other stages, the enhancement of the trades and the displacement of convection to the ITCZ area over the eastern tropical Pacific, characteristic of the mid-summer drought, diminishes rainfall. This study sets the stage for a better understanding of the mechanistic relationship between these weather types and rainfall characteristics in general, like onset, demise, and duration of rainy seasons. Hence, these results can inform process-based model diagnostics aiming at bias-correcting climate predictions at multiple timescales.

KEYWORDS

Central America, Weather Types, Precipitation, Convection patterns

1 | INTRODUCTION

The region constituted by Central America and southern Mexico (CA-SM) is a narrow land mass characterized by pronounced topography and surrounded by the tropical eastern tropical Pacific Ocean, the Caribbean Sea, and the Gulf of Mexico. The spatial variability of precipitation reflects the topography (Taylor and Alfaro, 2005; Muñoz-Jiménez et al., 2019). Here, local precipitation climatology relates to topography and its interaction with the atmospheric circulation (Amador et al., 2016a; 2016b) and its moisture transport from the adjacent oceans (Durán-Quesada et al., 2017; Morales et al., 2021). The main objective of this work is to inquire into the climatological relationship between atmospheric circulation and precipitation over the CA-SM region.

The climatological circulation over CA-SM is characterized by the seasonal migration of the North Atlantic subtropical high (NASH; Taylor and Alfaro, 2005; Martinez et al., 2019; Straffon et al., 2020) with its associated Caribbean Low-Level Jet (CLLJ; Amador, 1998; 2008; Cook and Vizy, 2010; Hidalgo et al., 2015; Durán-Quesada et al., 2017; Martinez et al., 2019; García-Martínez and Bollasina, 2020; Morales et al., 2021), the Inter-Tropical Convergence Zone (ITCZ; Adam et al., 2016a; 2016b) and the Choco jet (CJ; Poveda and Mesa, 2000). The seasonal migration and the modes of interaction between these mechanisms are related with the regional precipitation variability over CA-SM (Cook and Vizy, 2010; Hidalgo et al., 2015; Amador et al., 2016b; Durán-Quesada et al., 2017; García-Martínez and Bollasina, 2020; Mejía et al., 2021).

The CLLJ is an intermittent intense zonal flow (12–14 m·s^{-1}) over the Caribbean Sea, located between 925 and 700 hPa (García-Martínez and Bollasina, 2020) and characterized by an annual cycle with relative maxima during July and February and a minimum during October. The CLLJ is a moisture conveyor belt for Central America from the Caribbean Sea (Durán-Quesada et al., 2017; Morales et al., 2021) and it determines the position of the ITCZ over the eastern tropical Pacific on monthly time scales (Hidalgo et al., 2015).

The CJ is a southwesterly flow formed by the interaction between the cross-equatorial trade winds, the Pacific Ocean and the Andes (Poveda and Mesa, 2000; Espinoza et al., 2020; Cerón et al., 2021) and its annual maximum is during September, October, and November when it reaches further north supplying moisture to southern Central America and the ITCZ (Durán-Quesada et al., 2010; 2017; Mejía et al., 2021).

Interannual variability of precipitation in CA-SM is partly explained by the controls that variability modes of tropical Sea-Surface Temperature (SST) exert on the low-level wind fields (Durán-Quesada et al., 2017; Hidalgo et al., 2019). The main SST mode that influences the regional precipitation variability is El Niño–Southern Oscillation (ENSO; Trenberth, 1997; Waylen et al., 1996; Amador, 2008; Maldonado et al., 2013; 2018). This mode influences both the CLLJ (Amador, 1998; 2008; Hidalgo et al., 2019) and the CJ (Morales et al., 2021). These jets are also influenced by the tropical North Atlantic (TNA) SST (Alfaro, 2000; Maldonado et al., 2013; Hidalgo et al., 2015), the Pacific Decadal Oscillation (PDO; Mantua et al., 1997; Fallas-López and Alfaro, 2012) and the Atlantic Multidecadal Oscillation (AMO; Enfield et al., 2001; Maldonado et al., 2016). These large-scale teleconnections partially modulate the frequency of tropical cyclones in the region (e.g., Farfan et al., 2013; Martínez-Sanchez and Cavazos, 2014).

Regional climatology over the CA-SM is also partially modulated by the solstitial mode that connects the lower tropospheric circulation and precipitation (Wang et al., 2014) via the global monsoon (Trenberth et al., 2000; Geen et al., 2020). This mode peaks during July with significantly large amplitudes over this region and the adjacent tropical Pacific (Wang et al., 2014). However, Nie et al. (2010) found that during July the thermodynamic structure over this region does not meet the conditions for convective quasi-equilibrium (CQE; Arakawa and Schubert, 1974; Emanuel et al., 1994) that couple the circulation to large-scale convection and are normally associated with monsoons (Tomassini, 2020). According to Nie et al. (2010) for this time scale, moisture and temperature advection by regional circulation mechanisms may prevent this equilibrium.

Observational analysis of the precipitation climatology over Central America has shown that it can be represented by two annual regimes: a Pacific regime and a Caribbean regime (Alfaro, 2000). The Pacific regime that explains the 72% of the variability is composed of a dry season extending from (boreal) winter to early spring and a wet season during the remaining months, coherent with the solstitial mode from Wang et al., 2014. This rainy season is characterized by two precipitation maxima separated by a local minimum: the "canícula", "veranillo" or mid-summer drought (MSD; Magaña et al., 1999; Magaña and Caetano, 2005; Karnauskas et al., 2013; Alfaro, 2014; Maldonado et al., 2016; Alfaro and Hidalgo, 2017; Corrales-Suastegui et al., 2020; Zhao et al., 2020). The Caribbean regime that explains 8% of the variability is wet throughout the year, with mild seasonality featuring maxima during winter and summer, and minima during spring and autumn (Alfaro, 2000; Taylor and Alfaro, 2005).

On intraseasonal and shorter time scales, exogenous transient phenomena such as the Madden–Julian Oscillation (MJO; Madden and Julian, 1971; Barlow and Salstein, 2006; Barrett and Esquivel-Longoria, 2013; Poleo et al., 2014), easterly waves (Serra et al., 2010), tropical cyclones (Amador et al., 2010), upper-tropospheric troughs in westerlies (Fernández et al., 1996; Allen and Mapes,

2017), and cold surge intrusions from mid-latitudes (Henry, 1979; Schultz, 1998; Zárate-Hernández, 2013; Luna-Niño and Cavazos, 2017) are also important factors shaping the regional precipitation climatology. The forcing exerted by endogenous convection on the atmospheric circulation (Gill, 1980) over CA-SM has been reported for the cases of robust convection over the Pacific slopes of Colombia affecting the circulation in southern Central America and the Panamá Bight (Mesa-Sánchez and Rojo-Hernández, 2020; Mejía *et al.*, 2021), and of summer deep convection over Central America and surrounding oceans producing anomalous lower-tropospheric (upper-tropospheric) cyclonic (anti cyclonic) circulations over northern Central America, Mexico, and southwestern United States (Siu and Bowman, 2019; Chang *et al.*, 2021).

Following the outlined above, the working hypothesis is that rainfall variability in the CA-SM region is mostly driven by the interaction of SST variability modes, global modes, and regionally modulated mechanisms that impact low-level circulation, moisture transport, and thermal anomalies linked to convection. The main objective is to determine a finite set of recurrent regional circulation patterns or weather types (e.g., Ghil and Robertson, 2002) and relate these patterns with the major features of regional precipitation over the intra Americas seas. To accomplish this objective, we conduct a cross-time scale interference analysis (Muñoz *et al.*, 2015) connecting weather types (WT) with regional precipitation anomalies, atmospheric thermodynamic structures and climate variability modes. Weather type classifications had been successfully implemented to analyse the atmospheric circulation in the tropical Americas, resulting in circulation patterns that are characterized by a marked seasonality (Chadee and Clarke, 2015; Moron *et al.*, 2015; Sáenz and Durán-Quesada, 2015; Vigaud and Robertson, 2017; Gouirand *et al.*, 2020; Ochoa-Moya *et al.*, 2020).

Weather types are extracted from daily mean lower- and upper-tropospheric wind fields and convective available potential energy (CAPE). Lower-tropospheric circulation is preferred over sea level pressure because the circulation is far from geostrophic balance at these latitudes and these deviations may be relevant for CA-SM climate. Upper-tropospheric circulation is selected because it can be modified by exogenous mechanisms enhancing precipitation (Allen and Mapes, 2017) and endogenous convective forcing impacting the circulation (Siu and Bowman, 2019; Chang *et al.*, 2021). CAPE is included as a measure of regional instability and low-level moisture availability (Taszarek *et al.*, 2021) and has been successfully incorporated into seasonal climate prediction schemes over Central America (Alfaro *et al.*, 2018).

The thermodynamic structures related with WT are the contingent expected values of the equivalent potential temperature (θ_E) and saturation equivalent potential temperature (θ_E^S), which are used to assess the possible statistical thermodynamic coupling between lower and upper tropospheric levels that is characteristic of CQE, especially for rainy-season WT.

This paper follows with a description of the data and methods in section 2. In section 3.1 WT occurrence climatology, mean event duration and transition matrix are presented to assess WT temporal features. Section 3.2 presents the constitutive characteristics of WT by displaying the cluster centroids and, the expected mean low-level circulations and CAPE values. The relationships between WT and vertically integrated moisture flux divergence (VIMFD) and precipitation are addressed in section 3.3. In section 3.4 expected values for equivalent potential temperature anomalies and mean values are presented to describe the expected anomalous thermodynamic structures for each WT, a description of the relationships of the mean values of these variables with precipitation and circulation for the rainy-season WT is presented to inquire into the physical mechanisms underlying the rainy season stages. To relate relevant climate variability modes and WT frequencies, section 3.5 explores the relationship between WT occurrence and ENSO, TNA, and MJO related indexes. Section 4 features the discussion and in section 5 conclusions are provided.

2 | DATA AND METHODS

2.1 | Data

Gridded (30 km × 30 km) fields from ERA5 reanalysis (Hersbach *et al.*, 2020) for the period 1979–2019 were extracted for computing WT and their influence on VIMFD and thermodynamic structures: 6-hourly fields (0000, 0600, 1200, and 1800 UTC) of wind (925, 850, and 200 hPa levels), column CAPE, specific humidity, temperature, and geopotential height at 1000, 925, 850, 800, 700, 600, 400, 300, 250, 200, and 100 hPa levels. Vertically integrated moisture flux divergence was extracted at 1-hr resolution.

In the Central America and Caribbean regions ERA5 has been utilized with reasonable success in precipitation studies (Centella-Artola *et al.*, 2020; García-Franco *et al.*, 2020; García-Franco *et al.*, 2021; Giraldo-Cardenas *et al.*, 2021), in future projections of droughts and the CLLJ (Depsky and Pons, 2020; Vichot-Llano *et al.*, 2021, respectively), drought related issues (Pascale *et al.*, 2021; Stewart *et al.*, 2021) and in assessing the trends of the Caribbean trade wind inversion (Ramseyer and Miller, 2021).

A total of 174 rain gauges with daily rainfall observations from January 1979 to December 2010 (32 years) were used. For Central America, data were provided by the Meteorological Services in these countries and were

quality controlled according to guidelines issued by World Meteorological Organization (WMO 2010; 2014; 2018; 2019). This dataset has been employed in various regional studies (Maldonado *et al.*, 2016; 2017; Alfaro *et al.*, 2018).

For Mexico, data were provided by the Servicio Meteorológico Nacional and were quality controlled using Climate Computing software (CLIMCOM) developed by United Nations Organization and incorporated to Dunn *et al.* (2020) dataset.

From the total 174 available stations, 167 series have less than 15% of missing or suspicious data points, but 7 (4% of total) series with missing values ranging from 21 to 28% were included to provide spatial coverage over Honduras, where quality data are scarce. All the analysis described in section 2.2.3 were performed to unfilled data with no significant changes on the results. Time series were filled using the updated methodology from Alfaro and Soley (2009). This methodology fills datasets using PCA for filling groups of nearby or climatologically similar stations and auto regressive models for single series. No further quality control or homogeneity assessment has been performed to this dataset. A table with station metadata is provided as supplementary material.

In Central America, the spatial coverage of automatic weather stations is in decline (Quesada-Montano *et al.*, 2019). Here, the period with more availability of daily data is 1968–2012; however, as ERA5 starts in 1979 and only series with more than 85% of daily observation were allowed, the period that grants the greatest spatial coverage was 1979–2010. The spatial distribution of the rain gauges is shown in Figure 1.

Gridded precipitation data covering both ocean and land surfaces were obtained from PERSIANN-CDR dataset (Sorooshian *et al.*, 2014), these data were obtained for the period 1983–2019 on daily resolution in its native $0.25° \times 0.25°$ grid. This dataset was evaluated over Central America by Stewart *et al.* (2021) and performed reasonably well.

The relationships between WT occurrence and climate variability modes were analysed with respect to ENSO, TNA, and MJO. The following indices were used: Multivariate ENSO Index version 2 (MEIv2; Zhang *et al.*, 2019), Real-Time Multivariate MJO Index (RMM; Wheeler and Hendon, 2004), and the TNA index (Enfield and Alfaro, 1999).

2.2 | Methods

2.2.1 | Definition of weather types

Weather types were obtained by applying the *k*-means++ clustering algorithm from scikit-learn Python library (MacQueen, 1967; Lloyd, 1982; Arthur and Vassilvitskii, 2007; Pedregosa *et al.*, 2011) to daily wind fields at 925, 850, and 200 hPa, and CAPE.

Daily fields corresponded to means computed from 6-hourly data (0000, 0600, 1200, and 1800 UTC) for the geographical domain 106°–70°W and 5.5°–22.5°N. These data were converted into standardized anomalies, weighted by the cosine of the corresponding latitude (Chung and Nigam, 1999) and prefiltered in terms of their principal components (PC; Wilks, 2020). The leading 20 principal components (75% of the total variance) were retained after applying a North *et al.* (1982) test.

The number of clusters was selected as follows. A population of 200 normally distributed surrogate datasets with the same spectral features as the original data were obtained by applying the Fourier phase randomization
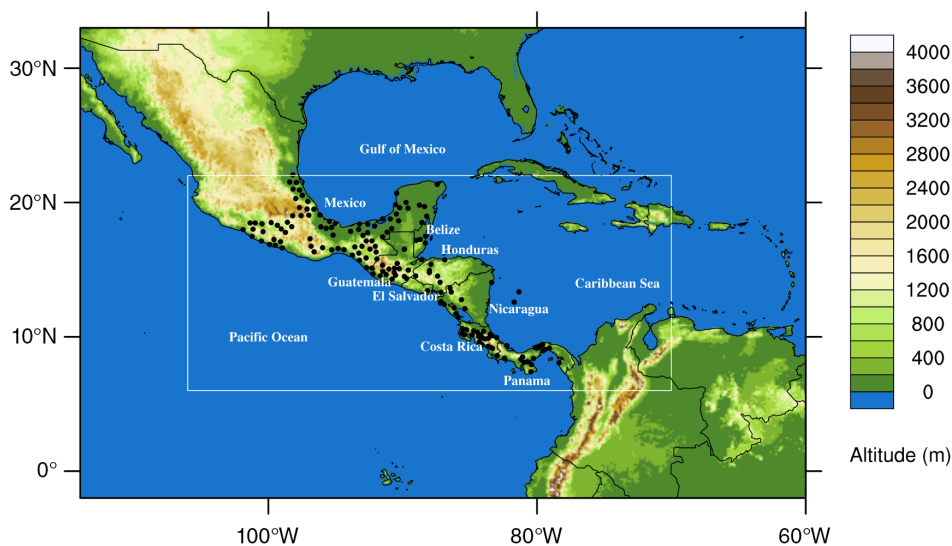

FIGURE 1 Geographical domain and gauge locations. In-box is the geographical domain of the Weather Typing method. Topographic data from ETOPO 1 (Amante and Eakins, 2009). Lake of Nicaragua was artificially drawn. [Colour figure can be viewed at wileyonlinelibrary.com]

technique (Theiler *et al.*, 1992) to data in PC space. For a series from 2 to 12 the *k*-means++ algorithm was executed 100 times to the original data, as well as for each of the 200 members of the surrogate data population and four metrics were computed: the classificability index (CI; Cheng and Wallace, 1993; Michelangeli *et al.*, 1995; Muñoz *et al.*, 2017), the mean-square-error (MSE), variance ratio criterion (VRC; Caliński and Harabasz, 1974), and Silhouette criterion (SC; Rousseeuw, 1987).

The optimal number of clusters was selected as the smallest value for which the following conditions were met:

$$CI_{data} > 0.99; MSE_{data} < P_{2.5\%}[MSE_{surr}];$$
$$VRC_{data} > P_{97.5\%}[VRC_{surr}]; \quad (1)$$
$$SC_{data} > P_{97.5\%}[SC_{surr}].$$

2.2.2 | Weather types: Spatiotemporal characteristics

Weather types were characterized by their climatology and expected values for standardized anomalies and for mean fields. The climatology of the probabilities of occurrence were computed and a Klee diagram (Muñoz *et al.*, 2015; 2017) plotted to visualize interannual variability. The transitions between WT were analysed by means of the daily transition matrix.

Spatial characteristics of WT were defined and discussed from the expected values of the standardized anomalies of wind vectors at 925 hPa and CAPE, as well as mean daily values of those variables and wind vectors at 200 hPa. Statistical significance for all expected values was assessed by means of *t* tests with 95% significance level.

Temporal ranges were selected to maximize sample sizes. Temporal changes in the frequency of WTs were evaluated by applying Mann–Kendall tests and no significant trends were found.

2.2.3 | Weather types and precipitation

The relationships between WT series and each precipitation series were established by means of categorical linear regressions using MATLAB software. Precipitation series were filtered with a low-pass filter with 9-days cut-off to filter out sub-synoptic variability. Weather type sequence was transformed into a multivariate dummy predictor variable. Each precipitation series was standardized and used as predictand. The regression coefficients represent expected values for each weather type and station.

Linear regression was chosen instead of conditional composites because the adjusted coefficients of variation represent the percentage of variability from each precipitation series that is accounted for by the classification.

2.2.4 | Vertically integrated moisture flux divergence and thermodynamic fields

The relationships between weather types and VIMFD, θ_E and θ_E^S were also analysed by means of categorical linear regressions for each grid point. Thermodynamic variables were computed from specific humidity, temperature, and geopotential height using the Bolton (1980) methods in Python library Metpy (May *et al.*, 2020). Before regressing, θ_E (θ_E^S) was vertically integrated from 1,000 to 600 hPa (400–200 hPa) and transformed to standardized anomalies.

2.2.5 | Climate variability modes

For analysing the ENSO influence we adapted the method of Muñoz *et al.* (2015). We selected the two seasons corresponding to the Pacific regime: from November to April (regional-scale dry season) and from May to October (wet season). For each season, the Spearman correlation between the seasonal mean MEIv2 index and the relative frequencies of weather types (typical of that season) were estimated. For analysing the effect of TNA, the same procedure as for ENSO was followed, changing the MEI index for the TNA index.

The influence of MJO events in the weather types occurrence was evaluated through the computation of conditional changes of the weather types frequencies upon the occurrence of MJO phases (RMM with amplitudes larger than one). These computations were done following a method employed by Cassou (2008), Riddle *et al.* (2013), and Muñoz *et al.* (2015) among others. It consists in applying Equation (2) to both the dry and the wet seasons as defined above,

$$C(WT, MJO) = 100 * \left[\frac{\left(\frac{N_{WT,MJO}}{N_{MJO}} - \frac{N_{WT}}{N_T} \right)}{\left(\frac{N_{WT}}{N_T} \right)} \right], \quad (2)$$

where N_T is the total number of days for the season in question, N_{WT} the number of days when a particular weather type is present (weather type = 1,...,*N*), N_{MJO} the number of days when the MJO was in a particular phase (MJO = 1,...,8), and $N_{WT,MJO}$ the number of days when a particular weather type and MJO phase were

simultaneously present. Statistical significance was assessed by constructing a null distribution for each of both seasonal C's by computing it for 10,000 random resamplings of the weather type sequence for each season.

3 | RESULTS

3.1 | Temporal features

The clustering procedure produced six WT, labelled from WT1 to WT6 according to the timing of its first dominant peak. The probabilities of occurrence are characterized by well-defined annual cycles (Figure 2). In a typical year, WT1, WT2, and WT3 dominate the regional climatology by occurring 97.5% of days from December through April while WT4, WT5, and WT6 dominate by occurring 87.9% of days from May through November. Hence, there are three regional circulation patterns for the Pacific dry season and three for Pacific wet season. The climatologies corresponding to WT1, WT2, WT3, and WT5 (WT4 and WT6) are unimodal (bimodal). Nonetheless, for WT6 the second peak of the climatology is almost 6 times larger than the first. The Klee diagram in Figure 3 shows that these climatologies feature great inter annual variability. In section 3.4 this is related with climate variability modes.

Figure 3 and Table 1 show that the duration of events varies among weather types. Dry season types: WT1, WT2, and WT3 tend to occur in shorter runs with mean lengths of 5, 4, and 5 days, respectively. Only WT1 occurred in an event persisting for more than 20 days. While wet season types: WT4, WT5, and WT6 tend to last

longer, with mean lengths of 9, 11, and 6, respectively. Types WT4 and WT5 tend to occur in long runs once or twice a year (Figure 3).

The transition matrix is presented in Table 1. In absolute terms, persistence dominates and only two types (WT1 and WT2) show transition probabilities greater than those expected by chance.

3.2 | Regional atmospheric circulation patterns

3.2.1 | Weather type centroids

This subsection analyses the WT in terms of their centroids emphasizing on the circulation at 925 hPa and CAPE. The expected values of the standardized anomalies (referred to as anomalies in the remaining text) of these variables are shown in Figure 4.

Type WT1 is characterized by northeasterly low-level anomalies, with CAPE anomalies that are negative over land and over the Caribbean while positive over the tropical eastern Pacific (Figure 4a).

Type WT2 features spatial patterns similar to those of WT1, but low-level wind anomalies over the Caribbean Sea and the isthmus are northwesterly, while over the Pacific, anomalies are northeasterly and stronger over the Tehuantepec and Papagayo Gaps (Figure 4b). Positive CAPE anomalies over the Pacific are displaced southward with respect to those under WT1.

Under WT3 nearly neutral low-level wind anomalies are found over the Caribbean Sea and some areas of the near Pacific Ocean, hence, there the circulation is close
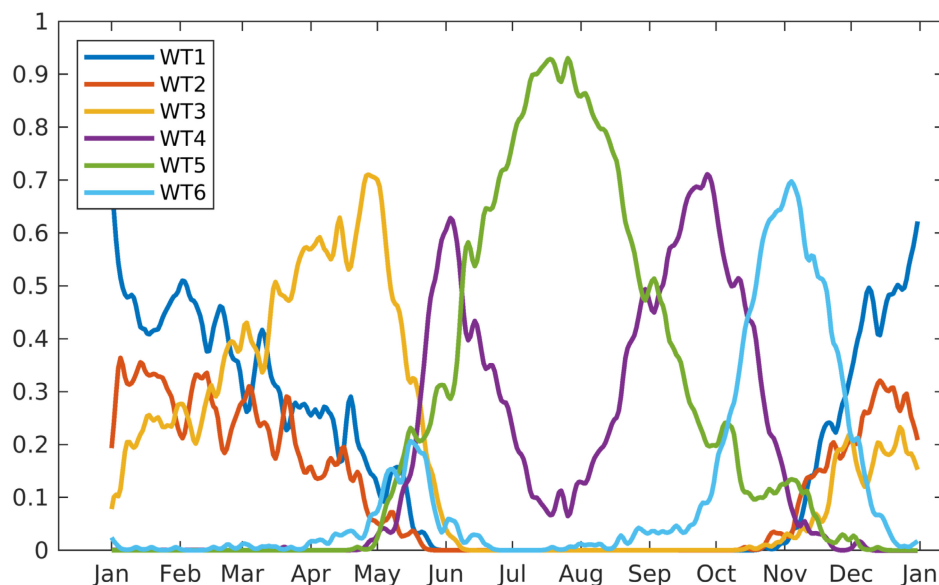

FIGURE 2   Climatology of observed occurrence probabilities for each weather type. Each line represents the probabilities of occurrence of each weather type on each Julian day and were smoothed with a 10-day moving average. [Colour figure can be viewed at wileyonlinelibrary.com]

FIGURE 3 Klee diagram. The horizontal axis represents each year from 1979 to 2019. Vertical axis represents the Julian days of each year. Colour scale represents the Weather Type present for each day. [Colour figure can be viewed at wileyonlinelibrary.com]
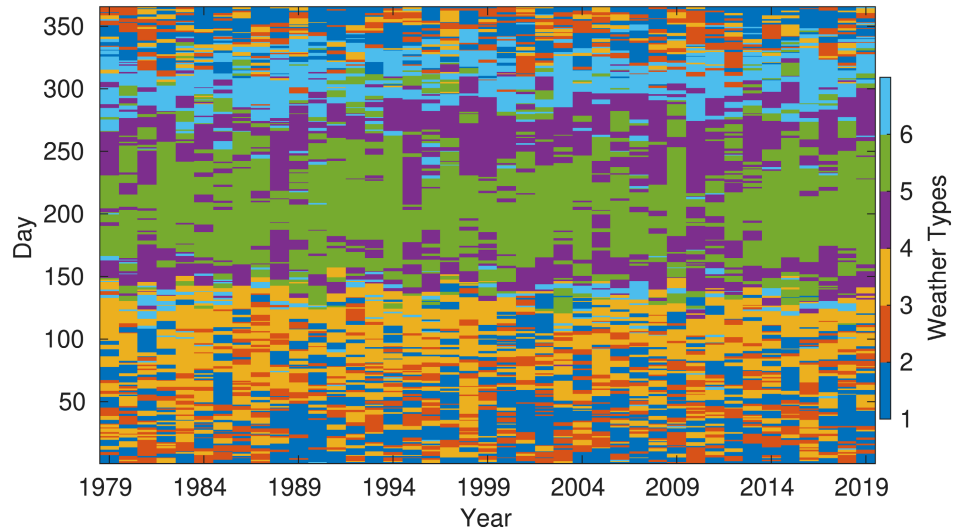

TABLE 1 Columns 2–7 show transition probabilities from WT in row to WT in column

	WT1	WT2	WT3	WT4	WT5	WT6	Mean run length
WT1	**75.3**	8.7	13.9	0.0	0.6	1.5	5.4
WT2	**21.9**	**63.5**	13.0	0.0	0.0	1.6	3.5
WT3	7.3	11.5	**74.1**	1.5	1.3	4.3	4.8
WT4	0.0	0.0	0.3	**85.2**	10.4	4.1	8.6
WT5	0.3	0.0	0.4	6.9	**89.4**	3.0	11.2
WT6	4.0	5.2	5.7	6.2	3.6	**75.3**	5.7

Note: Transitions occurring with probabilities above chance at the one-sided 95% level are bold typed (WT time series was shuffled 1,000 times to estimate the null distribution). Column 8 shows the mean length (days) of WT runs.
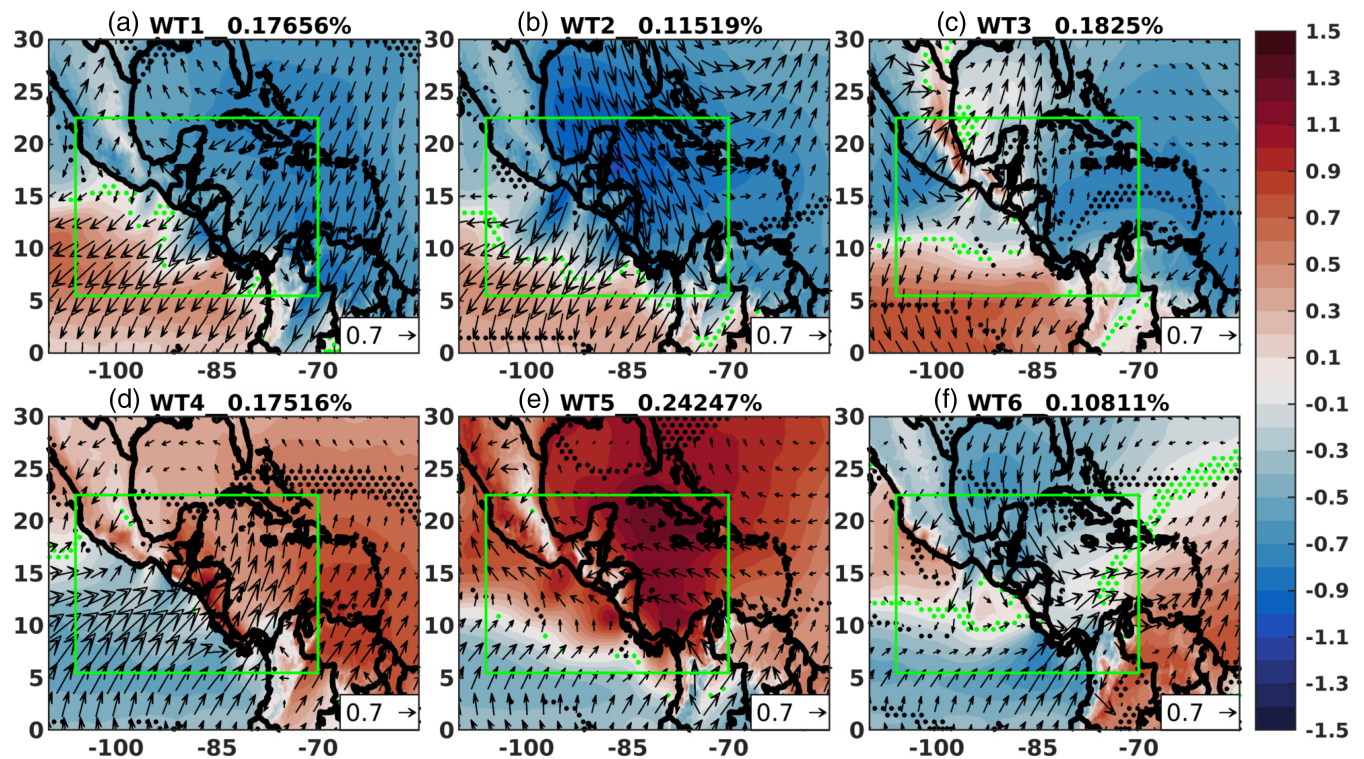

FIGURE 4 Composites of mean standardized anomalies for each WT. Vectors represent wind fields at 925 hPa vectors. Shaded contours represent CAPE. Dark (light) stippling indicate nonsignificant anomalies at 5% from a two-sided *t* test for wind fields (CAPE) [Colour figure can be viewed at wileyonlinelibrary.com]

to the climatological mean (Figure 4c). Northward low-level wind anomalies over Central America relate with reduced topographically induced flow ascent over the Caribbean slopes. CAPE anomalies remain negative over land except for coastal areas in the Gulf of Mexico and over Guatemala. Positive CAPE anomalies are at their largest values for the area south of 10°N over the eastern tropical Pacific.

Type WT4 features southwesterly anomalies over the whole area south of 15°N across the analysis domain (Figure 4d). These anomalies are part of an anomalous cyclonic circulation centred over Tehuantepec. CAPE anomalies feature positive values over land areas (with up to ~1 standard deviations over large portions of Honduras, Costa Rica, and Nicaragua) and the Caribbean Sea while over the eastern tropical Pacific anomalies are negative.

Under WT5 easterly anomalies over the Caribbean and Central America are characteristic, while over the eastern tropical Pacific anomalies are southeasterly near the coast, turning southwesterly south from 12°N (Figure 4e). CAPE anomalies are positive north of 12°N across the entire domain and are the largest among types, over the Caribbean Sea.

Type WT6 is characterized by large (~1 standard deviations) low-level northerly anomalies over land areas

north of 15°N that turn westerly over the Caribbean connecting to an anomalous cyclonic circulation centred northeast from Cuba (Figure 4f). Southwesterly anomalies from offshore the Pacific coast of Colombia cross the Isthmus south of 10°N. CAPE anomalies are mostly negative, except over offshore the Pacific coast of Mexico and northern South America (Venezuela).

3.2.2 | Expected mean daily circulations

This subsection analyses the expected values for the 925 and 200 hPa wind fields for each WT; Figures 5 and 6 show these fields. Type WT1 features a low-level circulation with enhanced trade winds (>15 m·s^{-1}) over the CLLJ region and Central America, this flow turns to the south crossing the Isthmus at the Papagayo and Panamá gaps, generating easterlies over the adjacent eastern tropical Pacific (Figure 5a). At 200 hPa, WT1 is characterized by a southwesterly flow connected with the mid-latitude westerlies (Figure 6a).

Under WT2, the 925 hPa circulation features northeasterly flow over the north Caribbean, land areas, and offshore the Pacific coasts, where it is enhanced by the Tehuantepec and Papagayo gaps. Convergence of this
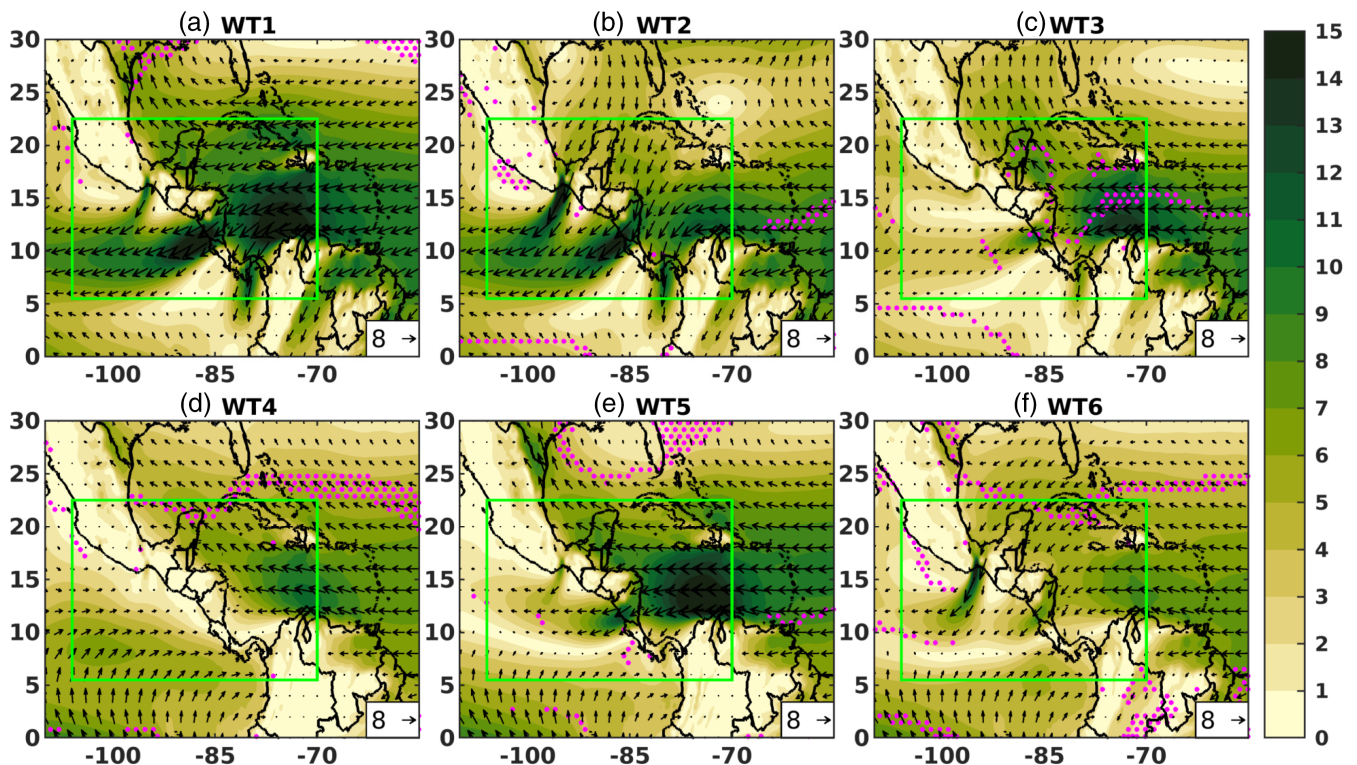

FIGURE 5 Composites of mean daily 925 hPa wind fields for each WT. Shaded contours represent wind speed in meters per second. Stippling indicate nonsignificant values at 5% from a two-sided *t* test [Colour figure can be viewed at wileyonlinelibrary.com]
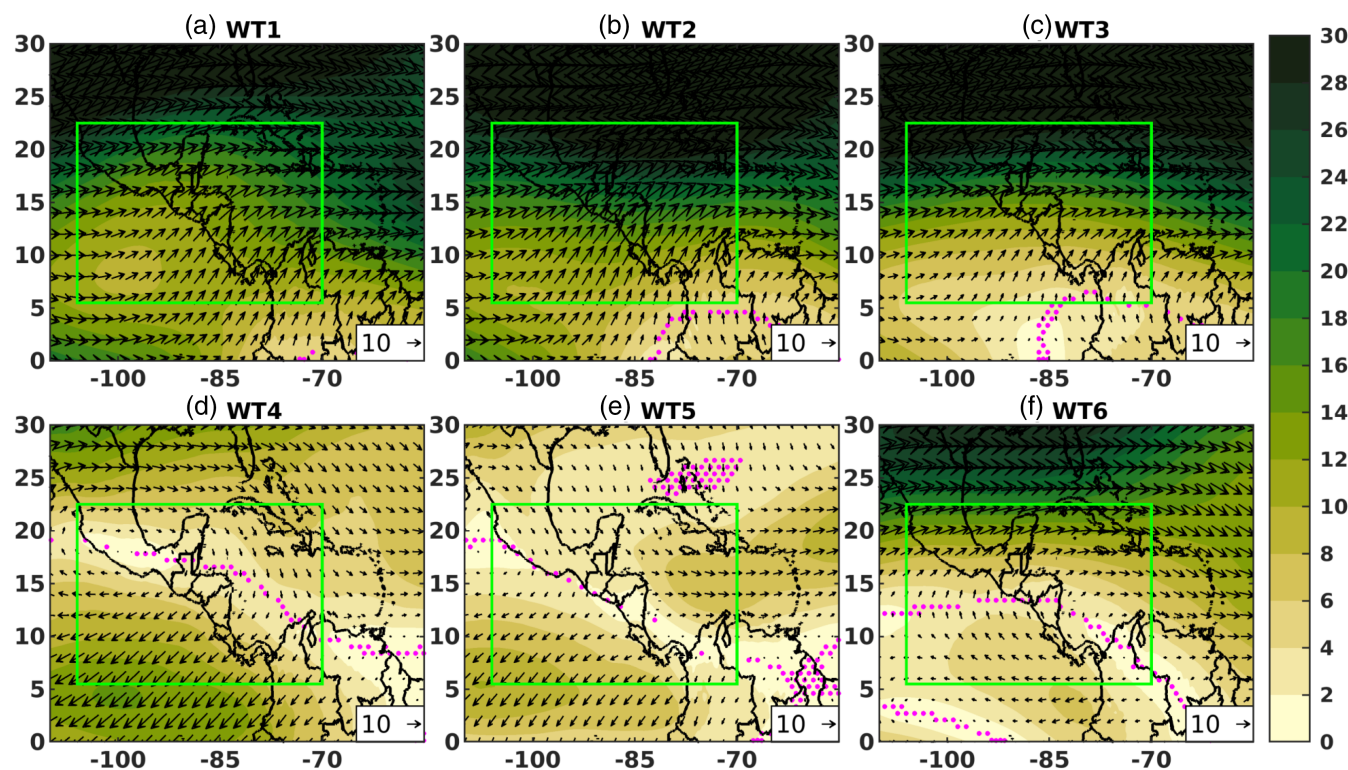
FIGURE 6 Composites of mean daily 200 hPa wind fields for each WT. Shaded contours represent wind speed in meters per second. Stippling indicate nonsignificant values at 5% from a two-sided *t* test [Colour figure can be viewed at wileyonlinelibrary.com]

flow with the trades forms a shear line over the southern Caribbean, off the coasts of Nicaragua and Costa Rica (Figure 5b). The circulation at 200 hPa features enhanced westerlies with respect to WT1, especially over northern Central America (Figure 6b).

As stated before, low-level circulation for WT3 is the closest among WT to the climatological mean over the Caribbean. Easterly winds are present over northern Costa Rica and Nicaragua while the remaining land areas of CA-SM feature wind speeds near zero (Figure 5c). Upper tropospheric circulation is similar to the contingent on WT1 (Figure 6c). Upper-level westerlies show a diminishing of the wave activity seen under WT1 and WT2.

For the rainy season circulations, WT4 features a suspension of the 925 hPa easterlies over Central America and the intrusion of the equatorial westerlies offshore Pacific coasts (Figure 5d). A cyclonic circulation centred over Tehuantepec is hinted by this figure but is clearly seen at the level 100 m above surface (see Figure 11). At 200 hPa, an anticyclonic circulation is formed above the low-level cyclone (Figure 6d). This atmospheric configuration is indicative of deep regional scale convection.

The 925 hPa level wind field under WT5 is characterized by a zonal flow larger than 15 m·s^{-1} over the CLLJ region, displaced slightly to the north with respect to the

maximum under WT1. This flow impacts Nicaragua and crosses the Isthmus at the Papagayo gap, with less intense gap winds than WT1. Most of CA-SM feature calm winds (Figure 5d). At 200 hPa, westerlies over the Caribbean are the slowest among all WT, an anticyclonic circulation is centred to the west of the characteristic of WT4 at the same latitude (Figure 6d).

Under WT6, 925 hPa level circulation shows calm (<5 m·s^{-1}) northeasterly flow over Central America converging with southerly flow from the Pacific over the southern extreme of the Caribbean. Gap winds are present southwest from Tehuantepec (Figure 5e). At 200 hPa, the mid-latitude westerlies are present over the northern parts of CA-SM, while an anticyclonic circulation is present to the south, centred above the low-level convergence mentioned above (Figure 6e).

3.2.3 | Expected mean daily CAPE values

This subsection presents the expected values of mean daily CAPE. In general, values are smaller over CA-SM than over adjacent oceanic areas. Under WT1 the largest CAPE values (approximately between 900 and 1,300 J·kg^{-1}) are found at the southern flank of the CLLJ and at the flanks of the gap wind areas over the Pacific, offshore Mexico, Costa Rica,
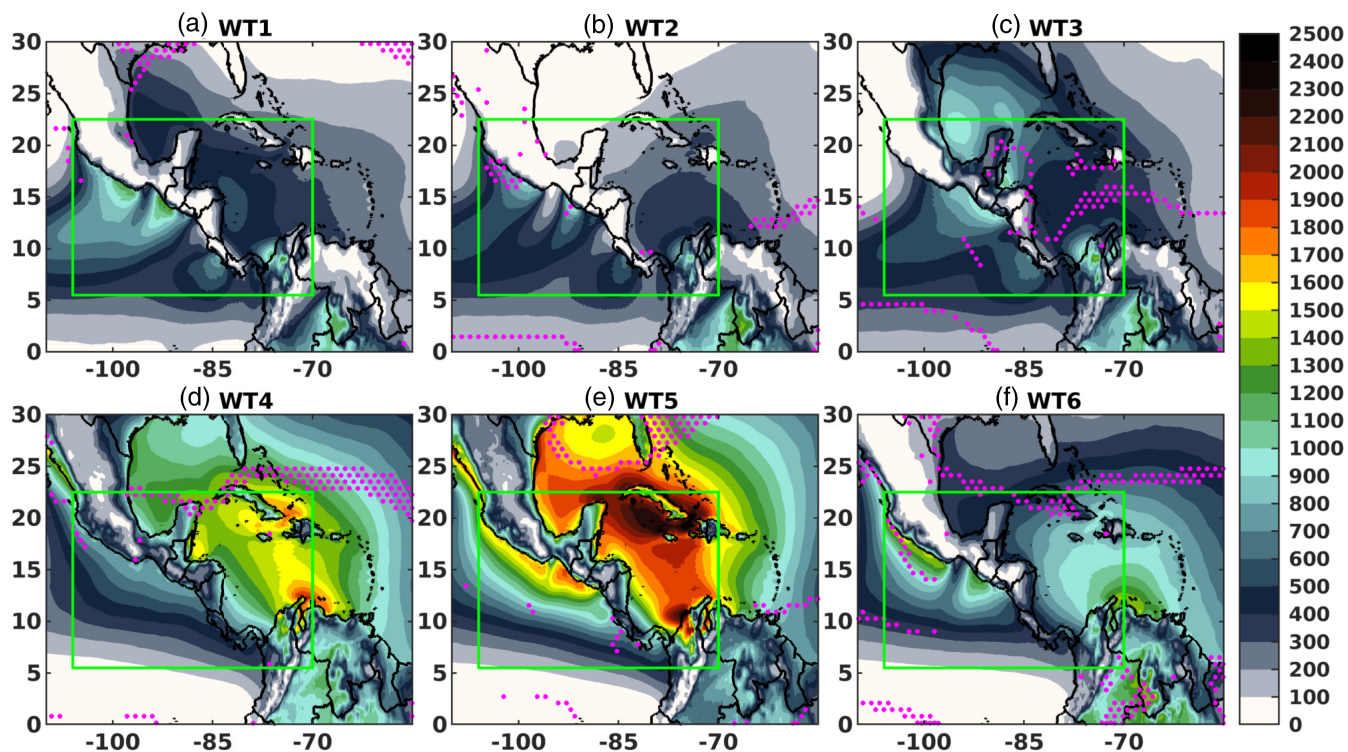
FIGURE 7 CAPE composites for each WT. Stippling indicate nonsignificant means at 5% from a two-sided *t* test (J·kg^{-1}) [Colour figure can be viewed at wileyonlinelibrary.com]

and Panamá coasts. Over CA-SM values are below 100 J·kg^{-1} (Figure 7a).

For WT2 the spatial distribution of the maxima is similar to that under WT1 but with smaller values (>800 J·kg^{-1}). A significant difference is that for WT2, CAPE values decrease from ~400 J·kg^{-1} to near 0 over the Gulf of Mexico (Figure 7b).

Under WT3 the largest CAPE (>1,000 J·kg^{-1}) is located at the southern flank of the CLLJ. Smaller values (~1,000 J·kg^{-1}) are found over the Gulf of Mexico and the Pacific Ocean near the coasts, from southern Mexico to El Salvador, with values reaching ~400 J·kg^{-1} over the land areas between these oceanic maxima (Figure 7c).

For the rainy season, CAPE values increase significantly with respect to dry season. Under wet season WT the spatial distribution of mean daily CAPE is skewed to the Caribbean. The largest CAPE values (~1,700 J·kg^{-1}) under WT4 are located near the Gulf of Venezuela and between Cuba and Hispaniola. Mean daily values over the entire Caribbean basin surpass 1,000 J·kg^{-1}, while over much of CA-SM CAPE is in the 500–1,000 J·kg^{-1} range (Figure 7d).

The spatial pattern of CAPE under WT5 is shaped similarly to that under WT4 over the Caribbean, but the values are the largest among all WT. Spatial maxima are located slightly westward from the correspondent to WT4, specifically west of Cuba and offshore from the

Caribbean coast of Colombia. These CAPE maxima reach 2,500 J·kg^{-1} while over the Caribbean basin values surpass 1,500 J·kg^{-1}. Large values (1,500 J·kg^{-1}) are also found over the Pacific coastal areas from Mexico to El Salvador (Figure 7e).

For WT6, CAPE values decrease significantly with respect to those under WT4 and WT5. Maxima reaches 1,500 J·kg^{-1} and are confined to a small area near the Gulf of Venezuela over the Caribbean and to the flanks of the Tehuantepec gap winds over the Pacific. Large areas of the Caribbean basin feature values near 1,000 J·kg^{-1} (Figure 7f).

3.3 | Vertically integrated moisture flux divergence and precipitation

This section analyses the spatial dependency of the relationships between the circulation represented by WT and moisture convergence and precipitation. Figure 8 shows the adjusted coefficients of determination (R adjusted) of each linear regression between WT and VIMFD at each grid-point (Figure 8a) and between WT and precipitation at each station (Figure 8b). R adjusted measures the variance of the dependent variable that is explained by the regression model.

The explanatory power of WT over low-passed (9 days) VIMFD is the largest (between 35 and 50% of the

FIGURE 8 Adjusted coefficients of determination (R-adjusted) from regressing weather types (as categorical time series) against daily standardized anomalies filtered with a low-pass filter (10 days cut-off) of VIMFD at each grid point (panel a) and precipitation at each station (panel b). Regression models for all grid-points and stations are significant at 99% (*F* test). These values reflect the strength of the linear relationship between weather types and the response variables [Colour figure can be viewed at wileyonlinelibrary.com]
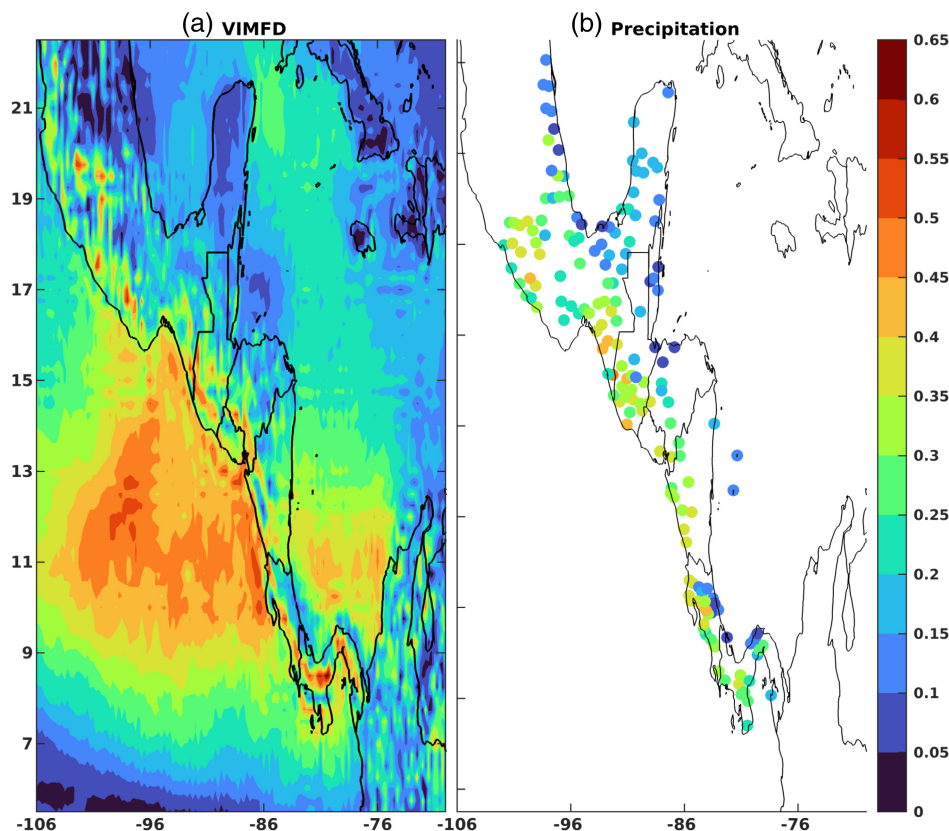
variability) along the Pacific coast of Central America, an adjacent oceanic area between 103°–85°W and 10°–15°N, and the western Caribbean between Nicaragua and Colombia (Figure 8a). Consistently, the explanatory power of WT over low-passed (9 days) precipitation is the largest (between 30 and 50% of the variability) along the Pacific coast of CA-SM. Hence, over the land, where the WT impact on VIMFD and precipitation coincide (Pacific slopes of CA-SM), the greater influence of WT classification on precipitation variability is explained by the former's capacity to partly explain the mechanisms of VIMFD variability.

Standardized precipitation anomalies under each WT are approximated by the regression coefficients shown in Figure 9. Weather types typical of boreal winter and spring (WT: 1–3) entail regional-scale dry conditions. Nonetheless, WT1 is associated with wet conditions along the Caribbean coast of Costa Rica (Figure 9a) while WT2 produces the wettest conditions along certain points of the Caribbean coasts of Honduras and Costa Rica (Figure 9b). Hence, enhanced trades (Figure 5a) are related with wet conditions over Caribbean slope coastal areas, while northeasterly flow (Figure 5b) produce wetter conditions over those areas via topographically forced ascent. Under WT3 there are the driest conditions along the Caribbean coasts and dry conditions elsewhere

(Figure 9c), these conditions are contingent of near zero 925 hPa wind anomalies over the Caribbean (Figure 4f).

Coefficients for WT typical of summer and autumn (WT: 4–6) entail mostly wet conditions. WT4 is associated with the wettest conditions along the Pacific slopes of CA-SM (Figure 9d). Wet conditions over northern areas of Central America are due associated with cyclonic anomalies inducing westerly flow (Figure 4d), while wet conditions to the south may be produced by moisture convergence and locally forced ascent. Dry conditions are present over the Caribbean areas of Costa Rica and Honduras.

Although WT5 is characterized by regional wet conditions, it is drier than WT4. Furthermore, dry conditions prevail over a small region along the Pacific coasts from northwest Costa Rica to southwest Honduras (Figure 9e). This spatial configuration, in conjunction with WT occurrence climatology, shows that WT5 represents the pattern of the MSD over the Pacific slopes of CA-SM. Recalling that the MSD constitutes a diminishing in rainfall and not a proper drought.

Precipitation anomalies under WT6 are characterized by dry conditions over the Pacific slopes of southern Mexico and Guatemala, and over the Caribbean coast of Costa Rica (Figure 9f). Wet conditions are present over the southern Gulf of Mexico mainly induced by north-easterly winds (Figure 5f), and over the Pacific coasts of
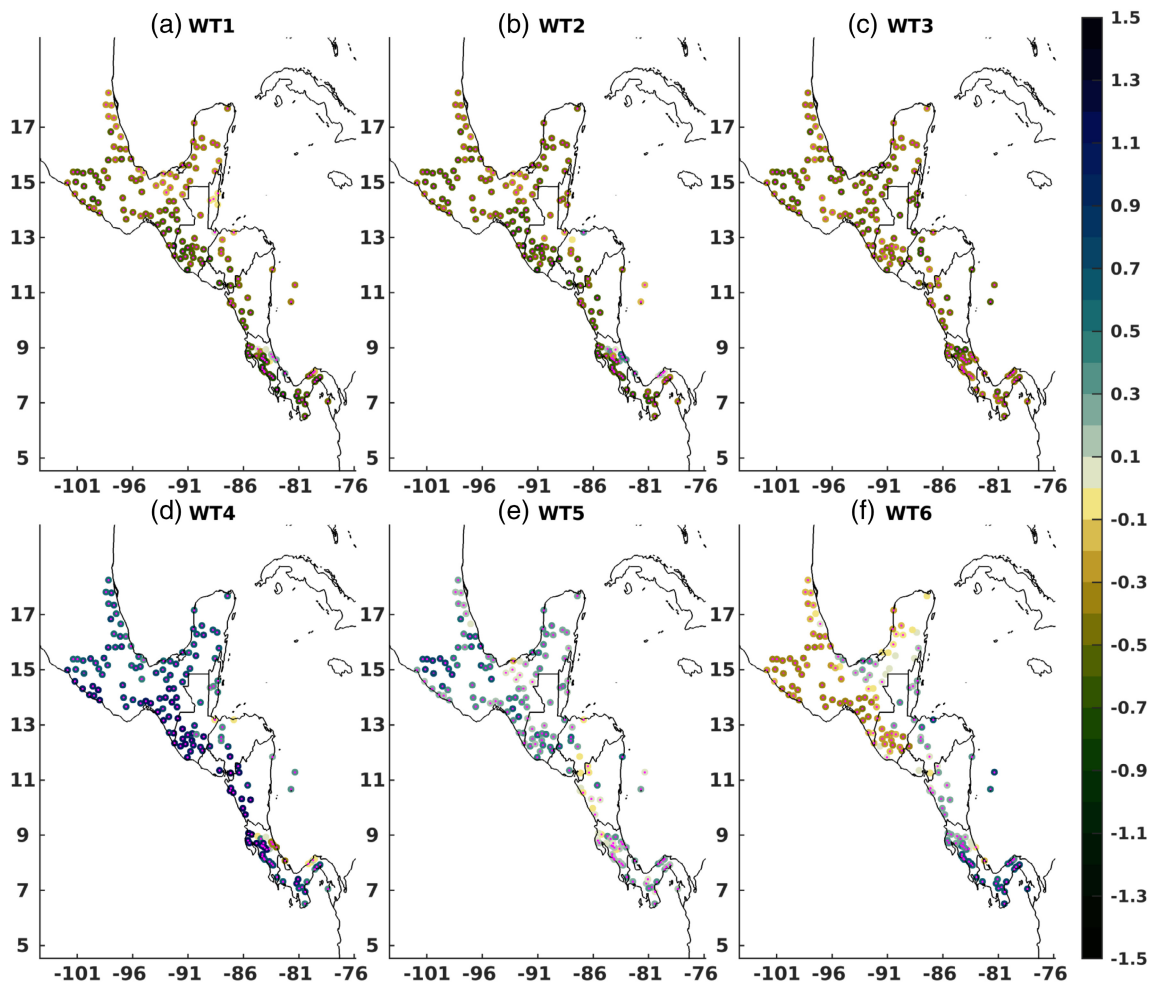
FIGURE 9 Regression coefficients from regressing weather types as categorical variable against standardized anomalies of precipitation at each station. These values represent the expected value of the standardized precipitation anomaly for each WT at each location. Stippling represent statistically significant coefficients at 95% [Colour figure can be viewed at wileyonlinelibrary.com]

Costa Rica and Panamá, where westerly low-level anomalies are linked to a cyclonic circulation (Figure 4f).

This analysis was also performed using CHIRPS data (Funk *et al.*, 2015), covering the period 1979–2019 resulting in consistent patterns (not shown).

3.4 | Thermodynamic structures

3.4.1 | Equivalent potential temperature anomalies

In this subsection the anomalous thermodynamic structures contingent on WT are analysed. The coefficients from regressing weather types against standardized anomalies of vertically integrated θ_E (1,000–600 hPa) and θ_E^S (400–200 hPa) for a domain containing most of tropical Americas are shown in Figure 10. Boreal winter and spring WT (WT: 1–3) are characterized by lower

troposphere cold patterns and suppressed convection over CA-SM, coherently with the negative anomalies of CAPE shown in Figure 5. Under WT2 large (~1.6) negative standardized anomalies are located over the Gulf of Mexico with the largest cold anomalies over CA-SM, resembling the spatial patterns associated with cold surge intrusions. An interesting feature is the magnitude of lower-tropospheric warm anomalies over South America and over the southern tropical eastern Pacific, especially between 5°S and the equator, under WT3 (Figure 10c). These are consistent with warm ENSO conditions.

The analysis of these structures is more relevant for the rainy season. Two weather types (WT4 and WT6) are characterized by anomalous fields in which maxima of θ_E and θ_E^S show covariability over certain regions, signalling an anomalous thermodynamic coupling mediated by convection. In the case of WT4, these maxima are found over the Yucatán peninsula (Figure 10d), under WT6 these are found over the Caribbean Sea (Figure 10f). For
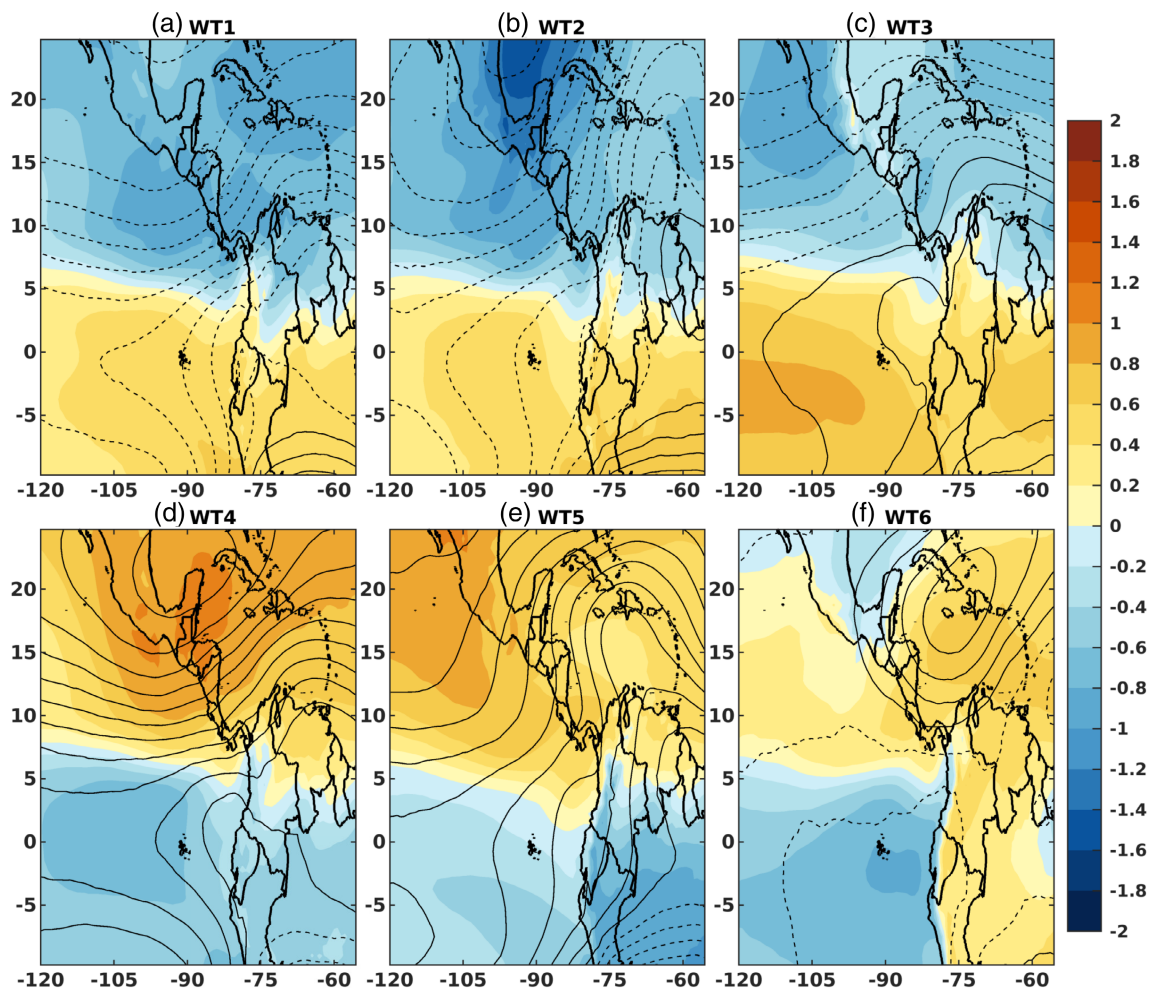
FIGURE 10   Regression coefficients from regressing weather types as categorical variable against standardized anomalies of equivalent potential temperature vertically integrated from 1000 to 600 hPa (shaded contours) and saturation equivalent potential temperature vertically integrated from 400 to 200 hPa (line contours). Values represent expected values of the standardized anomalies of each variable at each grid point for each WT [Colour figure can be viewed at wileyonlinelibrary.com]

WT5, there is a marked southeast to northwest thermal gradient from the Caribbean to the Gulf of California (Figure 10e).

3.4.2 | Mean thermodynamic structures and circulation under rainy season WT

This subsection analyses the expected values for θ_E and θ_E^S under WT4, WT5, and WT6; in conjunction with an analysis of streamlines at 100 m above the surface and precipitation from PERSIANN-CDR, to display a comprehensive vision of this variable (Figure 11).

Under WT4, low-level θ_E is maximum over the western flanks of the Sierra Madre del Sur (Figure 11a). Furthermore, θ_E over CA-SM is the warmest among rainy season WT, with relative maxima centered over Guatemala and western Colombia. Upper-tropospheric θ_E^S maximum is located slightly (~3°) to the west of the θ_E

absolute maximum. The atmospheric columns are thermodynamically coupled with the upper levels and strong convection is in statistical equilibrium with low-level thermal forcing (Figure 11a). Streamlines (100 m above surface) show convergence to the southeast of the θ_E maximum, while precipitation contours show a large area where daily mean values are greater than 10 mm·day^{-1} located to the south of the θ_E, θ_E^S, and convergence maxima.

For WT5 θ_E over CA-SM decreases nearly by 4 K with respect to the values under WT4. The absolute maximum is located over western Colombia and the Panamá bight and extends to the Pacific becoming a regional maximum, while the Sierra Madre del Sur maximum becomes relative. The upper-tropospheric θ_E^S maximum is displaced nearly 10° to the west (Figure 11b). An area of low-level convergence is located over the Panamá bight and extends to the Pacific where Atlantic, cross-equatorial south, and north, Pacific trades converge. Precipitation
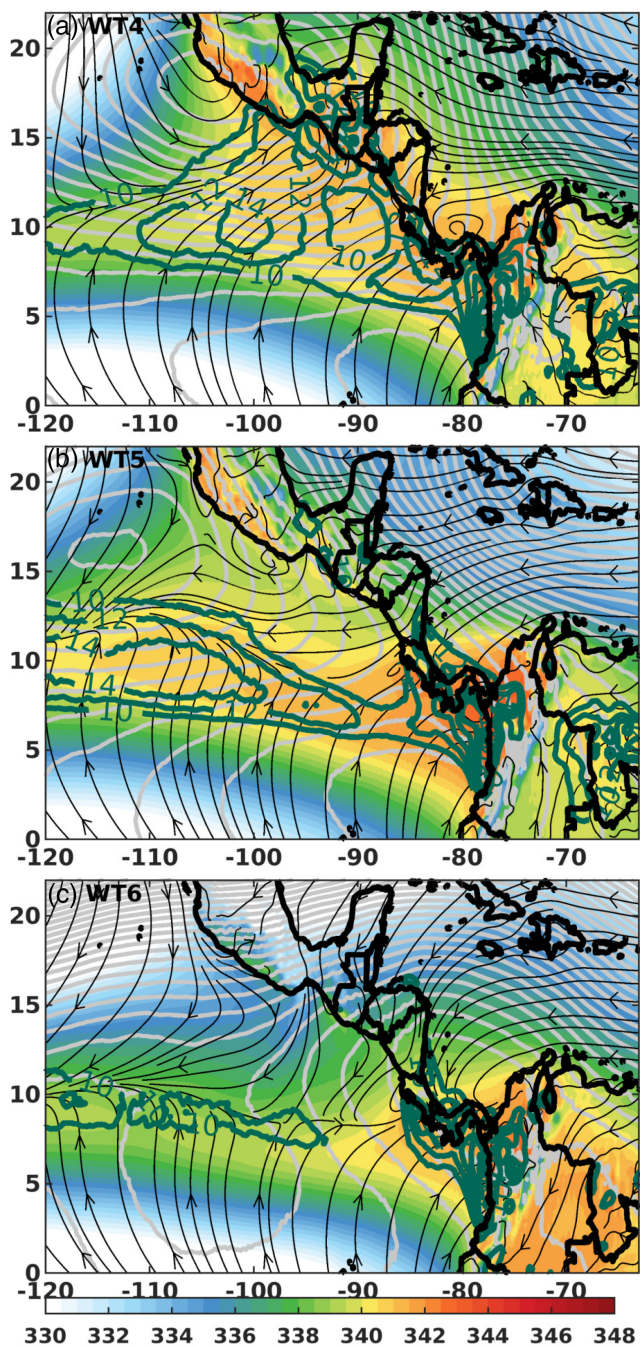
FIGURE 11 Thermodynamic structures, low-level circulation, and precipitation under wet WT. Equivalent potential temperature vertically integrated from 1000 to 600 hPa (shaded contours) [K], saturation equivalent potential temperature vertically integrated from 400 to 200 hPa (light contours) [K], stream lines 100 m above surface and PERSIANN-CDR mean daily precipitation greater (dark contours) than 10 mm·day^{-1} [Colour figure can be viewed at wileyonlinelibrary.com]

contours greater than 10 mm·day^{-1} are located on this convergence zone.

Under WT6, the maximum of low-level θ_E is located on western Colombia and the Panamá bight, with similar

(± 1 K) θ_E values over the other Colombian areas of the study domain. The relative maximum extends to the Pacific centred nearly at 10°N, with a decrease of ~6 K in 5° of latitude to north and south. The upper-tropospheric θ_E^S maximum is located over western Colombia, the Panamá bight and the southern Caribbean, thus strong convection is in statistical equilibrium with low-level thermal forcing (Figure 11c). Low-level convergence and precipitation greater than 10 mm·day^{-1} are colocated with the θ_E oceanic maximum.

3.5 | Climate variability indexes

3.5.1 | El Niño–Southern Oscillation

ENSO conditions, measured with MEIv2 index, influences the frequencies of occurrence of five WT. Specifically, WT characterized by zonal anomalies over the Caribbean, indifferently of the sign. Types WT1 (−0.44) and WT3 (0.68) present significant correlations (95%) with the MEIv2: during boreal winter, warm ENSO decreases the trades intensity producing drier conditions along the Caribbean coasts. The occurrence of WT2 is not modified by ENSO conditions.

During the wet season all WT have significant correlations with the MEIv2: WT4 (−0.76), WT5 (0.70), and WT6 (−0.31); for the last case the analysis encompasses the months of May and from September to December. Warm ENSO during summer is associated with an enhancement of the CLLJ (more WT5 days) and a reduction of westerly low-level flow over Central America, hence less WT4 and WT6 days.

3.5.2 | Tropical North Atlantic

In this analysis we replicated the procedure followed for ENSO using the TNA index. During the dry season only WT1 presents a significant correlation (−0.46): WT1 reflects an enhanced winter NASH that cools the ocean surface. During the wet season WT4 (0.51) and WT5 (−0.39) present significant correlations (95%). The former is related to anomalous subsidence allowing ocean surface heating over the Caribbean while the latter is associated with conditions similar to that of WT1.

3.5.3 | Madden–Julian Oscillation

In Figure 12 we show the relative changes in weather types frequencies contingent on MJO events. In general, WT characterized by enhanced zonal anomalies (WT1, WT4, and WT5) are more sensible to the occurrence of

FIGURE 12 Relative changes in weather types frequencies contingent on MJO events. These computations were done following a method employed by Cassou (2008), Riddle *et al*. (2013), and Muñoz *et al*. (2015) among others [Colour figure can be viewed at wileyonlinelibrary.com]
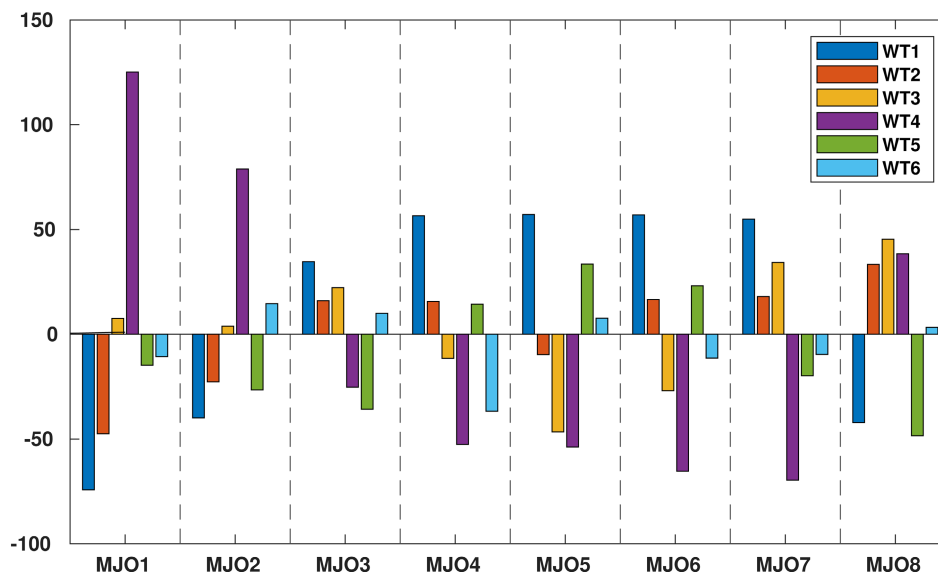
MJO events. Easterly phases of MJO (RMM phases 4, 5, and 6) are related with larger (smaller) than normal frequencies for WT1 and WT5 (WT4). While westerly phases of MJO (RMM phases 1, 2, and 8) are related to inverse frequency changes. To inquire for causal relationships, we produced a histogram of current and previous MJO conditions during the beginning of WT spells but found no significant relationship (not shown). Consequently, MJO events do not trigger WT spells.

4 | DISCUSSION

The weather type analysis applied to the wind and CAPE fields resulted in six WT that are taken as snapshots of the atmospheric circulation (Muñoz *et al*., 2015). This set of circulation patterns is characterized by a climatology of occurrence that is consistent with the precipitation climatology, particularly over the Pacific slopes of CA-SM.

The spatial relationship between WT and supra-synoptic precipitation was quantified by the R adjusted coefficients from the linear regression. The influences WT have on precipitation is more relevant over the Pacific coasts of Central America and southern Mexico (between 30 and 50% of the variability) than over the southern Gulf of Mexico and the Caribbean slopes (between 5 and 15% of the variability). Moreover, these regressions were repeated using the 11 circulation patterns from Sáenz and Durán-Quesada (2015) as regressor series, resulting in a similar spatial pattern with smaller (~0.1 less) R adjusted over the Pacific side and R adjusted between 5 and 20% over the Caribbean side. To address the lack of explanatory power over the Central American Caribbean slopes it is important to recall that these areas

are mostly wet throughout the year, with mild seasonality (Alfaro, 2000; Taylor and Alfaro, 2005). Furthermore, some studies (Biasutti *et al*., 2012; Rapp *et al*., 2014; Sáenz and Amador, 2016) have shown that over these areas the prevailing easterlies, the land–ocean breeze systems and the coastal curvatures interact to produce diurnal cycles of precipitation characterized by morning maxima in contrast with the adjacent Pacific slopes. These may be the reasons why the daily regional scale circulation patterns that are related with regional scale convection (or its absence) have no explanatory power for precipitation over a region full of complex local interactions.

The CA-SM Pacific side precipitation climatology can be described in terms of WT occurrence: three WT dominate the dry season (WT: 1–3), a wet pattern (WT6) that is more frequent during the transition phase, WT4 with its separated markedly bimodal distribution as that of the rainy season and WT5 long spells that represent the MSD. Dry and transition patterns tend to be less persistent (mean durations between 4 and 5 days) than wet season patterns (mean durations from 9 to 11 days). We proceed the discussion by analysing the correspondence between the unfolding of the WT climatology and the more relevant features of the regional atmospheric configurations and precipitation patterns, considering climate variability modes.

The canonical annual cycle of WT occurrence begins with an alternation between an enhanced-trades pattern (WT1) and a northerly low-level flow pattern (WT2), the latter is a transient state that commonly transitions to the former. Both are characterized by the lowest CAPE values over CA-SM, largest negative anomalies of θ_E and large negative precipitation anomalies, except for the Caribbean coast of Costa Rica. WT1 is interpreted as

constitutive of the winter maxima of the CLLJ with wind speeds larger than 15 m·s⁻¹ and featuring a negative correlation with ENSO, as does the CLLJ during boreal winter (Amador *et al.*, 2016a). This WT is also negatively correlated with TNA, because enhanced trades cool the sea surface.

Type WT2 resembles the "Winter North Cold Surge" pattern found by Sáenz and Durán-Quesada (2015), associated with the signal of a cold surge originated in Central Canada which enters the Gulf of Mexico and reaches further south (Henry, 1979; Schultz *et al.*, 1998; Zárate-Hernández, 2013). However, WT2 does not constitute an identifier for cold surges reaching Central America. For example, a comparison with the hand-made climatology for November–February of Zárate-Hernández (2013) suggests that using WT2 spells as cold surge intrusions underestimates the later by 52%. While a comparison with the cold surge climatology of Reding (1992) showed that WT2 spells were present in 70% of the 177 cold surges during the season from October to March in the 1979–1990 period and that both, WT1 and WT3, were present in ~50% of these events.

As the year unfolds WT3 becomes more frequent until it becomes dominant during April–May, WT3 is characterized by a circulation close to the climatological mean over the Caribbean, similar to the pattern typical of spring from Moron *et al.* (2015). The distribution of CAPE under WT3 displays larger values than those from WT1 and WT2, especially over Yucatán peninsula, the Gulf of Mexico coasts and adjacent ocean areas, probably because the southerly low-level anomalies produce anomalous moisture transport. Nonetheless, dry conditions are present across the entire domain. Regarding variability modes, WT3 is correlated (0.68) with ENSO, consistently with warm anomalies over the Southern Hemisphere tropical Pacific displayed by θ_E and neutral 925 hPa anomalies over the Caribbean. For warm (cold) ENSO phases occurring during boreal winter WT3 (WT1) becomes more frequent partially at the expense of WT1 (WT3), this implies less (more) days with enhanced winter CLLJ and drier (wetter) conditions over the Caribbean coast of Costa Rica.

Generally (31 out of 40 years), WT6 is the first wet type (see section 3.1 for an explanation of the enumeration). These WT6 spells tend to happen during May and are characterized by a reduction of the low-level easterlies and the influence of northerlies over the Pacific areas north of 12 N, which may reflect some cold surge intrusions. Under WT6, low-level thermal forcing is maximum over western Colombia, close to the Panamá border where the CQE conditions are found. Coherently with these conditions, the precipitation maximum is located equatorward of the θ_E maximum (Nie *et al.*, 2010). The reduced low-level

easterlies converge in a cyclonic circulation centred over the thermodynamically coupled area and an upper-tropospheric anticyclonic circulation is also observed. These circulations are a response, probably in Ekman balance, to the pressure gradients generated by convection. The ITCZ extends from this area to the Pacific nearly at 10°N. WT6 is characterized mostly by small precipitation anomalies (<0.3), negative over the Pacific slopes north of 11 N, Yucatán Peninsula, the western flanks of the Bahía de Campeche and the Caribbean coast of Costa Rica. Positive anomalies are large (~1 *SD*) over the South Pacific coast of Costa Rica and Panamá. This pattern is more frequent during cold ENSO events.

For WT4, which begins to occur during May and is dominant during June, September and October, analogous thermodynamics and dynamics to those under WT6 are present, but centred over the western flanks of the Sierra Madre del Sur. The building up of warm lower tropospheric air masses over land areas, especially over southern Mexico, generated by the northward march of the isolation maximum, produces an atmospheric response that reinforces the westerly flow reaching the Pacific slopes of Central America. Circulation anomalies at 925 hPa are similar to those reported by Zhao *et al.* (2020) for the period before the MSD onset. Anomalous subsidence outside the anomalous cyclonic circulation may contribute to the building of the thermal low over southern United States that García-Martínez and Bollasina (2020) propose as one of the forcing factors for CLLJ enhancement. This strengthening of the CLLJ is characteristic of the subsequent WT5 run.

Although the convection over the Panamá bight is not as organized as in the WT6 case, it is still present and connected with westerly flow inducing precipitation over the Pacific slopes of Costa Rica and Panamá. These conditions result in large (>1 *SD*) positive anomalies along the Pacific slopes from the Peninsula de Azuero in Panamá to the northern limit of the study domain in southern Mexico. The frequency of this WT strongly responds to ENSO, TNA, and MJO.

The midsummer climatology is dominated by WT5, which is characterized by the westward expansion of the NASH and the enhancement of the CLLJ. Although WT5 is characterized by the largest CAPE values among WT, there is no signs of organized convection occurring, except for over the Panamá bight and the southern extreme of the Caribbean, where low-level convergence is found. This convergence extends to the west forming the ITCZ over the tropical eastern Pacific. Subsidence and lower tropospheric (500 hPa–10 m) wind shear associated with the NASH inhibit convection across most of the domain but also generates CAPE by providing low-level moisture (Taszarek *et al.*, 2021). Under WT5 precipitation anomalies are small

(<1 *SD*) and mostly positive, except for the Pacific coasts of northern Costa Rica, Nicaragua, and Honduras. The frequency of wet days for WT5 is smaller than that of WT4 and for WT5 these may be related to the passage of easterly waves due to the enhanced CLLJ (Amador, 1998; Whitaker and Maloney, 2018) or travelling mesoscale convective systems formed at the southern flank of the CLLJ. Hence, WT5 corresponds with the signal of the MSD, featuring enhanced CLLJ and reduced convection. Furthermore, over the Pacific slopes from the Peninsula de Azuero in Panamá to southern Mexico the contrasts between WT4 and WT5 expected precipitation are the largest is the area with a persistent MSD (Maurer *et al.*, 2022).

After the period dominated by WT5, WT4 re-emerges to dominate the climatology during October, with a larger frequency of occurrence than during the first peak. The end of the rainy season, characterized by a southward displacement of precipitation is represented by the WT6 peak during November.

Furthermore, from the perspective of this analysis, the difference between both peaks of the rainy season (Straffon *et al.*, 2020; Martínez *et al.*, 2020) is due to the relative occurrences of WT4 and WT6. During its first peak in early May, the probability of occurrence of WT6 is nearly 0.2, in contrast with 0.6 of WT4 during its first peak in early June. During their second peaks (September for WT4 and late October for WT6), the probability of occurrence of both is nearly 0.7. While for interannual time scales, the interplay between WT4 and WT5 define the precipitation variability over the Pacific slopes. Both WT are largely influenced by ENSO and TNA and exhibit the largest variability among WT (not shown).

The discrepancies between rainy-season WT patterns of CAPE and of θ_E and θ_E^S can be explained with CQE theory. According to Arakawa and Schubert (1974), CQE is based on the premise that CAPE produced by large-scale motions is immediately consumed by moist convection and according to Emanuel (2007) CQE does not restrict the amount nor the variance of CAPE. Hence there is no reason to expect any direct relationship between mean daily CAPE and thermodynamic structures in areas of thermal coupling. However, for convective scales, results shown in Figure 7 are highly consistent, seasonally and regionally, with the average monthly lightning density values using data from the World Wide Lightning Location Network (WWLLN) for 2012–2020 (Amador and Arce-Fernández, 2022).

5 | CONCLUSIONS

The spatial patterns associated with the temporal variability of the circulation in the CA-SM are represented by six weather types. These are the building blocks of the regional variability structure, layered through the modulation by the annual cycle of solar isolation, and by the large-scale climate variability modes. By influencing the VIMFD, these WT modify the regional precipitation variability, especially over the Pacific slopes of CA-SM. Precipitation and associated VIMF in the Caribbean slopes are less influenced by regional scale circulations, where local factors, such as wind–topography interactions and transients, are more relevant and require further research.

The consistency between the thermodynamic structures, lower and upper-tropospheric circulations and precipitation under rainy season WT, provides an insight into the centres of thermodynamic forcing that are key for the climatological rainy season over the Pacific slopes of CA-SM. Principally, the distribution of lower-tropospheric θ_E over land areas. Given the spatial resolution of ERA5 and its satisfactory representation of precipitation patterns over the study region (Stewart *et al.*, 2021), this information is of great value for assessing regional climate model simulations in a physically meaningful way.

ORCID

Fernán Sáenz https://orcid.org/0000-0001-7100-6838
Hugo G. Hidalgo https://orcid.org/0000-0003-4638-0742
Ángel G. Muñoz https://orcid.org/0000-0002-2212-6654
Eric J. Alfaro https://orcid.org/0000-0001-9278-5017
Jorge A. Amador https://orcid.org/0000-0002-9407-9367
Jorge L. Vázquez-Aguirre https://orcid.org/0000-0001-7687-3877

REFERENCES

Adam, O., Bischoff, T. and Schneider, T. (2016a) Seasonal and inter-annual variations of the energy flux equator and ITCZ. Part I: zonally averaged ITCZ position. *Journal of Climate*, 29(9), 3219–3230. https://doi.org/10.1175/jcli-d-15-0512.1.

Adam, O., Bischoff, T. and Schneider, T. (2016b) Seasonal and interannual variations of the energy flux equator and ITCZ.

Part II: zonally varying shifts of the ITCZ. *Journal of Climate*, 29(20), 7281–7293. https://doi.org/10.1175/jcli-d-15-0710.1.

Alfaro, E.J. (2000) Some characteristics of the annual precipitation cycle in Central America and their relationships with its surrounding tropical oceans. *Topicos Meteorologicos y Oceanograficos*, 7(2), 99–115.

Alfaro, E.J. (2014) Caracterización del "veranillo" en dos cuencas de la vertiente del Pacífico de Costa Rica, America Central. *Revista de Biología Tropical*, 62(4), 1–15.

Alfaro, E.J., Chourio, X., Muñoz, Á.G. and Mason, S.J. (2018) Improved seasonal prediction skill of rainfall for the Primera season in Central America. *International Journal of Climatology*, 38, e255–e268. https://doi.org/10.1002/joc.5366.

Alfaro, E.J. and Hidalgo, H.G. (2017) Propuesta metodológica para la predicción climática estacional del veranillo en la cuenca del río Tempisque en el Pacífico Norte de Costa Rica. *Topicos Meteorologicos y Oceanograficos*, 16(1), 62–74.

Alfaro, E.J. and Soley, F.J. (2009) Descripción de dos métodos de rellenado de datos ausentes en series de tiempo meteorológicas. *Revista de Matemáticas: Teoría y Aplicaciones*, 19, 59–74.

Allen, T.L. and Mapes, B.E. (2017) The late spring Caribbean rainbelt: climatology and dynamics. *International Journal of Climatology*, 37(15), 4981–4993 10.1002/joc.5136.

Amador, J.A. (1998) A climatic feature of tropical americas. The trade wind easterly jet. *Topicos Meteorologicos y Oceanograficos*, 5(2), 91–102.

Amador, J.A. (2008) The intra-Americas sea low-level jet. *Annals of the New York Academy of Sciences*, 1146(1), 153–188. https://doi.org/10.1196/annals.1446.012.

Amador, J.A., Alfaro, E.J., Rivera, E. and Calderón, B. (2010) Climatic features and their relationship with tropical cyclones over the Intra-Americas seas. *Hurricanes and Climate Change*, 2, 149–173. https://doi.org/10.1007/978-90-481-9510-79.

Amador, J.A. and Arce-Fernández, D. (2022) WWLLN hot and cold-spots of lightning activity and their relation to climate in an extended Central America region 2012–2020. *Atmosphere*, 13(1), 76. https://doi.org/10.3390/atmos13010076.

Amador, J.A., Durán-Quesada, A.M., Rivera, E.R., Mora, G., Sáenz, F., Calderón, B. and Mora, N. (2016a) The easternmost tropical Pacific. Part II: seasonal and intraseasonal modes of atmospheric variability. *International Journal of Tropical Biology*, 64(1), 23.

Amador, J.A., Rivera, E.R., Durán-Quesada, A.M., Mora, G., Sáenz, F., Calderón, B. and Mora, N. (2016b) The easternmost tropical Pacific. Part I: a climate review. *International Journal of Tropical Biology*, 64(1), 1.

Amante, C. and Eakins, B.W. (2009) *ETOPO1 1 arc-minute global relief model: procedures, data sources and analysis.* Boulder, CO: National Geophysical Data Center, NOAA. NOAA technical memorandum NESDIS NGDC-24. https://doi.org/10.7289/V5C8276M.

Arakawa, A. and Schubert, W.H. (1974) Interaction of a cumulus cloud ensemble with the large-scale environment, Part I. *Journal of Atmospheric Sciences*, 31(3), 674–701.

Arthur, D. and Vassilvitskii, S. (2007). *K-means++: the advantages of careful seeding.* Paper presented at Proceedings of the Eighteenth Annual ACM-SIAM Symposium on Discrete Algorithms, Society for Industrial and Applied Mathematics, Philadelphia, PA, USA, SODA '07.

Barlow, M. and Salstein, D. (2006) Summertime influence of the Madden–Julian Oscillation on daily rainfall over Mexico and Central America. *Geophysical Research Letters*, 33, L21708. https://doi.org/10.1029/2006GL027738.

Barrett, B.S. and Esquivel-Longoria, M.I. (2013) Variability of precipitation and temperature in Guanajuato, Mexico. *Atmósfera*, 26(4), 521–536. https://doi.org/10.1016/S0187-6236(13)71093-2.

Biasutti, M., Yuter, S.E., Burleyson, C.D. and Sobel, A. (2012) Very high-resolution rainfall patterns measured by TRMM precipitation radar: seasonal and diurnal cycles. *Climate Dynamics*, 39, 239–258. https://doi.org/10.1007/s00382-011-1146-6.

Bolton, D. (1980) The computation of equivalent potential temperature. *Monthly Weather Review*, 108(7), 1046–1053. https://doi.org/10.1175/1520-0493(1980)108<1046:tcoept>2.0.co;2.

Caliński, T. and Harabasz, J. (1974) A dendrite method for cluster analysis. *Communications in Statistics*, 3(1), 1–27. https://doi.org/10.1080/03610927408827101.

Cassou, C. (2008) Intraseasonal interaction between the Madden–Julian Oscillation and the North Atlantic Oscillation. *Nature*, 455, 523–527. https://doi.org/10.1038/nature07286.

Centella-Artola, A., Bezanilla-Morlot, A., Taylor, M.A., Herrera, D. A., Martinez-Castro, D., Gouirand, I., Sierra-Lorenzo, M., Vichot-Llano, A., Stephenson, T., Fonseca, C., Campbell, J. and Alpizar, M. (2020) Evaluation of sixteen gridded precipitation datasets over the Caribbean region using gauge observations. *Atmosphere*, 11, 1334.

Cerón, W.L., Kayano, M.T., Andreoli, R.V., Avila-Diaz, A., de Souza, I.P. and Souza, R.A. (2021) Pacific and Atlantic multidecadal variability relations with the Choco and Caribbean low-level jets during the 1900–2015 period. *Atmosphere*, 12(9), 1120.

Chadee, X.T. and Clarke, R.M. (2015) Daily near-surface large-scale atmospheric circulation patterns over the wider Caribbean. *Climate Dynamics*, 44(11), 2927–2946. https://doi.org/10.1007/s00382-015-2621-2.

Chang, K., Bowman, K.P., Siu, L.W. and Rapp, A.D. (2021) Convective forcing of the North American monsoon anticyclone at intraseasonal and interannual time scales. *Journal of the Atmospheric Sciences*, 78(9), 2941–2956.

Cheng, X. and Wallace, J.M. (1993) Cluster analysis of the northern hemisphere wintertime 500-hpa height field: spatial patterns. *Journal of the Atmospheric Sciences*, 50(16), 2674–2696. https://doi.org/10.1175/1520-0469(1993)050h2674:CAOTNHi2.0.CO;2.

Chung, C. and Nigam, S. (1999) Weighting of geophysical data in principal component analysis. *Journal of Geophysical Research: Atmospheres*, 104(D14), 16925–16928. https://doi.org/10.1029/1999JD900234.

Cook, K.H. and Vizy, E.K. (2010) Hydrodynamics of the Caribbean low-level jet and its relationship to precipitation. *Journal of Climate*, 23(6), 1477–1494. https://doi.org/10.1175/2009JCLI3210.1.

Corrales-Suastegui, A., Fuentes-Franco, R. and Pavia, E.G. (2020) The mid-summer drought over Mexico and Central America in the 21st century. *International Journal of Climatology*, 40, 1703–1715. https://doi.org/10.1002/joc.6296.

Depsky, N. and Pons, D. (2020) Meteorological droughts are projected to worsen in Central America's dry corridor throughout the 21st century. *Environmental Research Letters*, 16(1), 014001.

Dunn, R.J.H., Alexander, L.V., Donat, M.G., Zhang, X., Bador, M., Herold, N., Lippmann, T., Allan, R., Aguilar, E., Barry, A.A.,

Brunet, M., Caesar, J., Chagnaud, G., Cheng, V., Cinco, T., Durre, I., Guzman, R., Htay, T.M., Wan Ibadullah, W.M. and Bin Hj Yussof, M.N. (2020) Development of an updated global land in situ-based data set of temperature and precipitation extremes: HadEX3. *Journal of Geophysical Research: Atmospheres*, 125(16). https://doi.org/10.1029/2019jd032263.

Durán-Quesada, A.M., Gimeno, L. and Amador, J.A. (2017) Role of moisture transport for Central American precipitation. *Earth System Dynamics*, 8(1), 147–161. https://doi.org/10.5194/esd-8-147-2017.

Durán-Quesada, A.M., Gimeno, L., Amador, J.A. and Nieto, R. (2010) Moisture sources for Central America: identification of moisture sources using a lagrangian analysis technique. *Journal of Geophysical Research*, 115(D5), D05103. https://doi.org/10.1029/2009JD012455.

Emanuel, K. (2007) Quasi-equilibrium dynamics of the tropical atmosphere. *The Global Circulation of the Atmosphere*, 186–218.

Emanuel, K.A., David Neelin, J. and Bretherton, C.S. (1994) On large-scale circulations in convecting atmospheres. *Quarterly Journal of the Royal Meteorological Society*, 120(519), 1111–1143. https://doi.org/10.1002/qj.49712051902.

Enfield, D.B. and Alfaro, E.J. (1999) The dependence of Caribbean rainfall on the interaction of the tropical Atlantic and Pacific oceans. *Journal of Climate*, 12(7), 2093–2103. https://doi.org/10.1175/1520-0442(1999)012h2093:TDOCROi2.0.CO;2.

Enfield, D.B., Mestas-Nuñez, A.M. and Trimble, P.J. (2001) The Atlantic multidecadal oscillation and its relation to rainfall and river flows in the continental U.S. *Geophysical Research Letters*, 28(10), 2077–2080. https://doi.org/10.1029/2000GL012745.

Espinoza, J.C., Garreaud, R., Poveda, G., Arias, P.A., Molina-Carpio, J., Masiokas, M., Viale, M. and Scaff, L. (2020) Hydroclimate of the Andes, part I: main climatic features. *Frontiers in Earth Science*, 8. https://doi.org/10.3389/feart.2020.00064.

Fallas-López, B. and Alfaro, E.J. (2012) Uso de herramientas estadísticas para la predicción estacional del campo de precipitación en América Central como apoyo a los Foros Climáticos Regionales. 1: Análisis de tablas de contingencia. *Revista de Climatología*, 12, 61–79.

Farfan, L.M., Alfaro, E. and Cavazos, T. (2013) Characteristics of tropical cyclones making landfall on the Pacific coast of Mexico: 1970–2010. *Atmosfera*, 26(2), 163–182.

Fernández, W., Chacón, R.E. and Magarejo, J.W. (1996) On the rainfall distribution with altitude over Costa Rica. *Revista Geofisica*, 44, 56–72.

Funk, C., Peterson, P., Landsfeld, M., Pedreros, D., Verdin, J., Shukla, S., Husak, G., Rowland, J., Harrison, L., Hoell, A. and Michaelsen, J. (2015) The climate hazards infrared precipitation with stations—a new environmental record for monitoring extremes. *Sci Data*, 2, 150066. https://doi.org/10.1038/sdata.2015.66.

García-Franco, J.L., Gray, L.J. and Osprey, S. (2020) The American monsoon system in HadGEM3. 0 and UKESM1 CMIP6 simulations. *Weather and Climate Dynamics Discussions*, 2020, 1–33.

García-Franco, J.L., Osprey, S. and Gray, L.J. (2021) A wavelet transform method to determine monsoon onset and retreat from precipitation time-series. *International Journal of Climatology*, 41(11), 5295–5317.

García-Martínez, I.M. and Bollasina, M.A. (2020) Sub-monthly evolution of the Caribbean low-level jet and its relationship with regional precipitation and atmospheric circulation. *Climate Dynamics*, 54, 4423–4440.

Geen, R., Bordoni, S., Battisti, D.S. and Hui, K. (2020) Monsoons, ITCZs, and the concept of the global monsoon. *Reviews of Geophysics*, 58, e2020RG000700. https://doi.org/10.1029/2020RG000700.

Ghil, M. and Robertson, A.W. (2002) "Waves" vs. "particles" in the atmosphere's phase space: a pathway to long-range forecasting? *Proceedings of the National Academy of Sciences of the United States of America*, 99, 2493–2500. https://doi.org/10.1073/pnas.012580899.

Gill, A.E. (1980) Some simple solutions for heat-induced tropical circulation. *Quarterly Journal of the Royal Meteorological Society*, 106(449), 447–462. https://doi.org/10.1002/qj.49710644905.

Giraldo-Cardenas, S., Arias, P.A., Vieira, S.C. and Zuluaga, M.D. (2021) Easterly waves and precipitation over northern South America and the Caribbean. *International Journal of Climatology*, 42, 1483–1499.

Gouirand, I., Moron, V. and Sing, B. (2020) Seasonal atmospheric transitions in the Caribbean basin and Central America. *Climate Dynamics*, 55, 1809–1828. https://doi.org/10.1007/s00382-020-05356-6.

Henry, W.K. (1979) Some aspects of the fate of cold fronts in the Gulf of Mexico. *Monthly Weather Review*, 107, 1078–1082. https://doi.org/10.1175/1520-0493(1979)107<1078:SAOTFO>2.0.CO;2.

Hersbach, H., Bell, B., Berrisford, P., Hirahara, S., Horányi, A., Muñoz-Sabater, J., Nicolas, J., Peubey, C., Radu, R., Schepers, D., Simmons, A., Soci, C., Abdalla, S., Abellan, X., Balsamo, G., Bechtold, P., Biavati, G., Bidlot, J., Bonavita, M., Chiara, G., Dahlgren, P., Dee, D., Diamantakis, M., Dragani, R., Flemming, J., Forbes, R., Fuentes, M., Geer, A., Haimberger, L., Healy, S., Hogan, R.J., Hólm, E., Janisková, M., Keeley, S., Laloyaux, P., Lopez, P., Lupu, C., Radnoti, G., Rosnay, P., Rozum, I., Vamborg, F., Villaume, S. and Thépaut, J.N. (2020) The ERA5 global reanalysis. *Quarterly Journal of the Royal Meteorological Society*, 146, 1999–2049. https://doi.org/10.1002/qj.3803.

Hidalgo, H.G., Alfaro, E.J., Amador, J.A. and Bastidas, A. (2019) Precursors of quasi-decadal dry-spells in the Central America Dry Corridor. *Climate Dynamics*, 53(3–4), 1307–1322. https://doi.org/10.1007/s00382-019-04638-y.

Hidalgo, H.G., Durán-Quesada, A.M., Amador, J.A. and Alfaro, E.J. (2015) The Caribbean low-level jet, the inter-tropical convergence zone and precipitation patterns in the Intra-Americas Sea: a proposed dynamical mechanism. *Geografiska Annaler: Series A, Physical Geography*, 97(1), 41–59. https://doi.org/10.1111/geoa.12085.

Karnauskas, K.B., Seager, R., Giannini, A. and Busalacchi, A. (2013) A simple mechanism for the climatological midsummer drought along the Pacific coast of Central America. *Atmosfera*, 26(25), 261–281.

Lloyd, S. (1982) Least squares quantization in pcm. *IEEE Transactions on Information Theory*, 28(2), 129–137. https://doi.org/10.1109/TIT.1982.1056489.

Luna-Niño, R. and Cavazos, T. (2017) Formation of a coastal barrier jet in the Gulf of Mexico due to the interaction of cold fronts with the Sierra Madre Oriental mountain range. *Quarterly*

Journal of Royal Meteorological Society, 144, 115–128. https://doi.org/10.1002/qj.3188.

MacQueen, J. (1967) Some methods for classification and analysis of multivariate observations. In: *Proceedings of the Fifth Berkeley Symposium on Mathematical Statistics and Probability: Statistics*, Vol. 1. Berkeley, CA: University of California Press, pp. 281–297.

Madden, R.A. and Julian, P.R. (1971) Detection of a 40–50 day oscillation in the zonal wind in the tropical Pacific. *Journal of the Atmospheric Sciences*, 28, 702–708.

Magaña, V., Amador, A. and Medina, S. (1999) The midsummer drought over Mexico and Central America. *Journal of Climate*, 12, 1577–1588.

Magaña, V. and Caetano, E. (2005) Temporal evolution of summer convective activity over the Americas warm pools. *Geophysical Research Letters*, 32, L02803. https://doi.org/10.1029/2004GL021033.

Maldonado, T., Alfaro, E., Rutgersson, A. and Amador, J.A. (2017) The early rainy season in Central America: the role of the tropical North Atlantic SSTs. *International Journal of Climatology*, 37, 3731–3742. https://doi.org/10.1002/joc.4958.

Maldonado, T., Alfaro, E.J., Fallas-López, B. and Alvarado, L. (2013) Seasonal prediction of extreme precipitation events and frequency of rainy days over Costa Rica, Central America, using canonical correlation analysis. *Advances in Geosciences*, 33, 41–52. https://doi.org/10.5194/adgeo-33-41-2013.

Maldonado, T., Alfaro, E.J. and Hidalgo, H.G. (2018) A review of the main drivers and variability of Central America's climate and seasonal forecast systems. *International Journal of Tropical Biology*, 66(1), 153. https://doi.org/10.15517/rbt.v66i1.33294.

Maldonado, T., Rutgersson, A., Alfaro, E., Amador, J. and Claremar, B. (2016) Interannual variability of the midsummer drought in Central America and the connection with sea surface temperatures. *Advances in Geosciences*, 42, 35–50. https://doi.org/10.5194/adgeo-42-35-2016.

Mantua, N.J., Hare, S.R., Zhang, Y., Wallace, J.M. and Francis, R.C. (1997) A Pacific interdecadal climate oscillation with impacts on Salmon production. *Bulletin of the American Meteorological Society*, 78(6), 1069–1080.

Martinez, C., Goddard, L., Kushnir, Y. and Ting, M. (2019) Seasonal climatology and dynamical mechanisms of rainfall in the Caribbean. *Climate Dynamics*, 53(1), 825–846. https://doi.org/10.1007/s00382-019-04616-4.

Martínez-Sanchez, J.N. and Cavazos, T. (2014) Eastern tropical Pacific hurricane variability and landfalls on Mexican coasts. *Climate Research*, 58, 221–234.

Martínez, C., Kushnir, Y., Goddard, L. and Ting, M. (2020) Interannual variability of the early and late-rainy seasons in the Caribbean. *Climate Dynamics*, 55(5–6), 1563–1583. https://doi.org/10.1007/s00382-020-05341-z.

May, R.M., Arms, S.C., Marsh, P., Bruning, E., Leeman, J.R., Goebbert, K., Thielen, J.E. and Bruick, Z. (2020) *MetPy: a python package for meteorological data*. Boulder, CO: Unidata. Available at: https://github.com/Unidata/MetPy. https://doi.org/10.5065/D6WW7G29.

Maurer, E.P., Stewart, I.T., Joseph, K. and Hidalgo, H.G. (2022) The Mesoamerican mid-summer drought: the impact of its definition on occurrences and recent changes. *Hydrology and Earth System Sciences*, 26(5), 1425–1437. https://doi.org/10.5194/hess-26-1425-2022.

Mejía, J.F., Yepes, J., Henao, J.J., Poveda, G., Zuluaga, M.D., Raymond, D.J. and Fuchs-Stone, Ž. (2021) Towards a mechanistic understanding of precipitation over the far eastern tropical Pacific and western Colombia, one of the rainiest spots on Earth. *Journal of Geophysical Research: Atmospheres*, 126(5), e2020JD033415.

Mesa-Sánchez, D. and Rojo-Hernández, O. (2020) On the general circulation of the atmosphere around Colombia. *Revista de la Academia Colombiana de Ciencias Exactas, Físicas y Naturales*, 44(172), 857–875.

Michelangeli, P., Vautard, R. and Legras, B. (1995) Weather regimes: recurrence and quasi stationarity. *Journal of Atmospheric Sciences*, 52(8), 1237–1256.

Morales, J.S., Arias, P.A., Martínez, J.A. and Durán-Quesada, A.M. (2021) The role of low-level circulation on water vapour transport to central and northern South America: insights from a 2D Lagrangian approach. *International Journal of Climatology*, 41, E2662–E2682.

Moron, V., Gouirand, I. and Taylor, M. (2015) Weather types across the Caribbean basin and their relationship with rainfall and sea surface temperature. *Climate Dynamics*, 47(1), 601–621. https://doi.org/10.1007/s00382-015-2858-9.

Muñoz, Á.G., Goddard, L., Robertson, A.W., Kushnir, Y. and Baethgen, W. (2015) Cross-time scale interactions and rainfall extreme events in southeastern South America for the austral summer. Part I: potential predictors. *Journal of Climate*, 28(19), 7894–7913. https://doi.org/10.1175/JCLI-D-14-00693.1.

Muñoz, Á.G., Yang, X., Vecchi, G.A., Robertson, A.W. and Cooke, W.F. (2017) A weather-type-based cross-time-scale diagnostic framework for coupled circulation models. *Journal of Climate*, 30(22), 8951–8972. https://doi.org/10.1175/JCLI-D-17-0115.1.

Muñoz-Jiménez, R., Giraldo-Osorio, J.D., Brenes-Torres, A., Avendaño-Flores, I., Nauditt, A., Hidalgo-León, H.G. and Birkel, C. (2019) Spatial and temporal patterns, trends and teleconnection of cumulative rainfall deficits across Central America. *International Journal of Climatology*, 39, 1940–1953. https://doi.org/10.1002/joc.5925.

Nie, J., Boos, W.R. and Kuang, Z. (2010) Observational evaluation of a convective quasi-equilibrium view of monsoons. *Journal of Climate*, 23(16), 4416–4428. https://doi.org/10.1175/2010JCLI3505.1.

North, G.R., Bell, T.L., Cahalan, R.F. and Moeng, F.J. (1982) Sampling errors in the estimation of empirical orthogonal functions. *Monthly Weather Review*, 110, 669–706.

Ochoa-Moya, C.A., Cala-Pérez, Y.A., Díaz-Esteban, Y., Castro, C.L., Ordoñez-Peréz, P. and Quintanar, A.I. (2020) Climatological large-scale circulation patterns over the Middle Americas region. *Atmosphere*, 11(7), 745. https://doi.org/10.3390/atmos11070745.

Pascale, S., Kapnick, S.B., Delworth, T.L., Hidalgo, H.G. and Cooke, W.F. (2021) Natural variability vs forced signal in the 2015–2019 Central American drought. *Climatic Change*, 168(3), 1–21.

Pedregosa, F., Varoquaux, G., Gramfort, A., Michel, V., Thirion, B., Grisel, O., Blondel, M., Prettenhofer, P., Weiss, R., Dubourg, V. and Vanderplas, J. (2011) Scikit-learn: machine

learning in python. *Journal of Machine Learning Research.*, 12, 2825–2830.

Poleo, D., Solano-León, E. and Stolz, W. (2014) La Oscilación atmosférica Madden–Julian (MJO) y las lluvias en Costa Rica. *Tópicos Meteorológicos y Oceanográficos*, 13, 58.

Poveda, G. and Mesa, O.J. (2000) On the existence of Lloró (the rainiest locality on Earth): Enhanced ocean–land–atmosphere interaction by low-level jet. *Geophysical Research Letters*, 27(11), 1675–1678. https://doi.org/10.1029/1999GL006091.

Quesada-Montano, B., Wetterhall, F., Westerberg, I.K., Hidalgo, H. G. and Halldin, S. (2019) Characterising droughts in Central America with uncertain hydro-meteorological data. *Theoretical and Applied Climatology*, 137, 2125–2138. https://doi.org/10.1007/s00704-018-2730-z.

Ramseyer, C.A. and Miller, P.W. (2021) Historical trends in the trade wind inversion in the tropical North Atlantic Ocean and Caribbean. *International Journal of Climatology*, 41(12), 5752–5765.

Rapp, A.D., Peterson, A.G., Frauenfeld, O.W., Quiring, S.M. and Roark, E.B. (2014) Climatology of storm characteristics in Costa Rica using the TRMM precipitation radar. *Journal of Hydrometeorology*, 15(6), 2615–2633.

Reding, P.J. (1992) *The Central American cold surge: An observational analysis of the deep southward penetration of the North American cold fronts*. Master's thesis, Texas A&M University.

Riddle, E.E., Stoner, M.B., Johnson, N.C., L'Heureux, M.L., Collins, D.C. and Feldstein, S.B. (2013) The impact of the MJO on clusters of wintertime circulation anomalies over the North American region. *Climate Dynamics*, 40, 1749–1766. https://doi.org/10.1007/s00382-012-1493-y.

Rousseeuw, P.J. (1987) Silhouettes: a graphical aid to the interpretation and validation of cluster analysis. *Journal of Computational and Applied Mathematics*, 20, 53–65. https://doi.org/10.1016/0377-0427(87)90125-7.

Sáenz, F. and Amador, J.A. (2016) Características del ciclo diurno de precipitación en el Caribe de Costa Rica. *Revista de Climatología*, 16, 21–34 (in spanish).

Sáenz, F. and Durán-Quesada, A.M. (2015) A climatology of low level wind regimes over Central America using a weather type classification approach. *Frontiers in Earth Sciences*, 3, 15. https://doi.org/10.3389/feart.2015.00015.

Schultz, D.M., Bracken, W.E. and Bosart, L.F. (1998) Planetary and synoptic scale signatures associated with Central American cold surges. *Monthly Weather Review*, 126(1), 5–27. https://doi.org/10.1175/1520-0493(1998)126h0005:PASSSAi2.0.CO;2.

Serra, Y.L., Kiladis, G.N. and Hodges, K.I. (2010) Tracking and mean structure of easterly waves over the Intra-Americas Sea. *Journal of Climate*, 23(18), 4823–4840. https://doi.org/10.1175/2010JCLI3223.1.

Siu, L.W. and Bowman, K.P. (2019) Forcing of the upper-tropospheric monsoon anticyclones. *Journal of the Atmospheric Sciences*, 76(7), 1937–1954.

Stewart, I.T., Maurer, E.P., Stahl, K. and Joseph, K. (2021) Recent evidence for warmer and drier growing seasons in climate sensitive regions of Central America from multiple global datasets. *International Journal of Climatology*, 42, 1399–1417. https://doi.org/10.1002/joc.7310.

Straffon, A., Zavala-Hidalgo, J. and Estrada, F. (2020) Preconditioning of the precipitation interannual variability in southern Mexico and Central America by oceanic and atmospheric anomalies. *International Journal of Climatology*, 40, 3906–3921. https://doi.org/10.1002/joc.6434.

Sorooshian, S., Nguyen, P., Sellars, S., Braithwaite, D., AghaKouchak, A. and Hsu, K. (2014) Satellite-based remote sensing estimation of precipitation for early warning systems. *Extreme Natural Hazards, Disaster Risks and Societal Implications*, 99–112. https://doi.org/10.1017/cbo9781139523905.011.

Taszarek, M., Allen, J.T., Marchio, M. and Brooks, H.E. (2021) Global climatology and trends in convective environments from ERA5 and rawinsonde data. *npj Climate and Atmospheric Science*, 4, 35. https://doi.org/10.1038/s41612-021-00190-x.

Taylor, M.A. and Alfaro, E.J. (2005) Central America and the Caribbean, climate of. In: Oliver, J.E. (Ed.) *Encyclopedia of World Climatology. Encyclopedia of Earth Sciences Series*. Dordrecht: Springer. https://doi.org/10.1007/1-4020-3266-8_37.

Theiler, J., Eubank, S., Longtin, A., Galdrikian, B. and Farmer, J.D. (1992) Testing for nonlinearity in time series: the method of surrogate data. *Physica D: Nonlinear Phenomena*, 58(1), 77–94.

Tomassini, L. (2020) The interaction between moist convection and the atmospheric circulation in the Tropics. *Bulletin of the American Meteorological Society*, 101(8), E1378–E1396. https://doi.org/10.1175/BAMS-D-19-0180.1.

Trenberth, K.E. (1997) The definition of El Niño. *Bulletin of the American Meteorological Society*, 78(12), 2771–2778.

Trenberth, K.E., Stepaniak, D.P. and Caron, J.M. (2000) The global monsoon as seen through the divergent atmospheric circulation. *Journal of Climate*, 13(22), 3969–3993. https://doi.org/10.1175/1520-0442(2000)013<3969:tgmast>2.0.co;2.

Vichot-Llano, A., Martinez-Castro, D., Bezanilla-Morlot, A., Centella-Artola, A., Gil-Reyes, L., Torres-Alavez, J.A., Corrales-Suastegui, A. and Giorgi, F. (2021) Caribbean low-level jet future projections using a multiparameter ensemble of RegCM4 configurations. *International Journal of Climatology*, 42, 1544–1559. https://doi.org/10.1002/joc.7319.

Vigaud, N. and Robertson, A. (2017) Convection regimes and tropical-midlatitude interactions over the intra-American seas from May to November. *International Journal of Climatology*, 37(S1), 987–1000. https://doi.org/10.1002/joc.5051.

Wang, P.X., Wang, B., Cheng, H., Fasullo, J., Guo, Z.T., Kiefer, T. and Liu, Z.Y. (2014) The global monsoon across timescales: coherent variability of regional monsoons. *Climate of the Past*, 10, 2007–2052.

Waylen, P.R., Caviedes, C.N. and Quesada, M.E. (1996) Interannual variability of monthly precipitation in Costa Rica. *Journal of Climate*, 9(10), 2606–2613. https://doi.org/10.1175/1520-0442(1996)009h2606:IVOMPIi2.0.CO;2.

Wheeler, M.C. and Hendon, H.H. (2004) An all-season real-time multivariate MJO index: development of an index for monitoring and prediction. *Monthly Weather Review*, 132(8), 1917–1932.

Whitaker, J.W. and Maloney, E.D. (2018) Influence of the Madden–Julian oscillation and Caribbean low-level jet on East Pacific easterly wave dynamics. *Journal of the Atmospheric Sciences*, 75, 1121–1141.

Wilks, D. (2020) *Statistical Methods in the Atmospheric Sciences*. Amsterdam, Netherlands: Elsevier.

WMO. (2010) *Guide to the Global Observing System*. Geneva: World Meteorological Organization.

WMO. (2014) *Guide to Instruments and Methods of Observation.* Geneva: World Meteorological Organization.

WMO. (2018) *Guide to Climatological Practices.* Geneva: World Meteorological Organization.

WMO. (2019) *Manual on the Global Data-Processing and Forecasting System. Annex IV to the WMO Technical Regulations.* Geneva: World Meteorological Organization.

Zárate-Hernández, E. (2013) Climatología de masas invernales de aire frío que alcanzan Centroamérica y el caribe y su relación con algunos índices árticos. *Tópicos meteorológicos y oceanográficos*, 12(1), 35–55.

Zhao, Z., Holbrook, N.J., Oliver, E.C., Ballestero, D. and Vargas-Hernandez, J.M. (2020) Characteristic atmospheric states during mid-summer droughts over Central America and Mexico. *Climate Dynamics*, 55, 681–701. https://doi.org/10.1007/s00382-020-05283-6.

Zhang, T., Hoell, A., Perlwitz, J., Eischeid, J., Murray, D., Hoerling, M. and Hamill, T.M. (2019) Towards probabilistic multivariate ENSO monitoring. *Geophysical Research Letters*, 46(17–18), 10532–10540. https://doi.org/10.1029/2019gl083946.

Zuo, J., Li, W., Sun, C. and Ren, H.C. (2019) Remote forcing of the northern tropical Atlantic SST anomalies on the western North Pacific anomalous anticyclone. *Climate Dynamics*, 52, 2837–2853. https://doi.org/10.1007/s00382-018-4298-9.

SUPPORTING INFORMATION

Additional supporting information can be found online in the Supporting Information section at the end of this article.